IEEE Access
Multidisciplinary ⋮ Rapid Review ⋮ Open Access Journal

Received 28 July 2023, accepted 25 August 2023, date of publication 4 September 2023, date of current version 13 September 2023.

Digital Object Identifier 10.1109/ACCESS.2023.3311626

RESEARCH ARTICLE

ASO-Based SHE Method on Hybrid Multilevel Inverter for PV Application Under Dynamic Operating Conditions

PEEYUSH KALA[1], (Member, IEEE), VIBHU JATELY[2], (Senior Member, IEEE), ABHINAV SHARMA[2], JYOTI JOSHI[3], AND BRIAN AZZOPARDI[4,5], (Senior Member, IEEE)

[1]Department of Electrical and Electronics Engineering, SRM Institute of Science and Technology, Delhi NCR Campus, Ghaziabad 201204, India
[2]Department of Electrical and Electronics Engineering, University of Petroleum and Energy Studies, Dehradun 248007, India
[3]Department of Computer Science and Engineering, Graphic Era Hill University, Dehradun 248002, India
[4]Institute of Engineering and Transport, Malta College of Arts, Science and Technology (MCAST), PLA9032 Paola, Malta
[5]The Foundation for Innovation and Research–Malta, BKR4012 Birkirkara, Malta

Corresponding author: Vibhu Jately (vibhujately@gmail.com)

This work is supported in part by the European Commission H2020 TWINNING JUMP2Excel (Joint Universal activities for Mediterranean PV integration Excellence) project under grant 810809.

Funded by the European Union

Partly funded by the European Union under Grant 101079469 PROMISE ''Photovoltaics Reliability Operations and Maintenance Innovative Solutions for Energy Alliance'' project.

ABSTRACT In multilevel inverters (MLI), output voltage waveform consists of dominant low order harmonics, which needs to be minimized. Simultaneously, good control over the fundamental voltage for desirable operation is needed. In this paper, an atom search optimization (ASO) based selective harmonic elimination (SHE) method is proposed for a variable dc bus based reduced component count (RCC) MLI. ASO is a population-based metaheuristic algorithm, which mathematically models the motion of atoms in nature to accurately determine the optimum firing angle of the switches by solving SHE fitness function. The proposed ASO SHE method outperforms recent metaheuristics based SHE methods such as bee algorithm, imperialistic colonial algorithm (ICA), firefly, particle swarm optimization (PSO), and teaching learning-based optimization (TLBO) in solving SHE problem for 11-level multilevel inverter. Detailed simulation case studies are presented to effectively demonstrate the performance of the proposed ASO SHE method on a stand-alone photovoltaic (PV) based RCC MLI subjected to sudden changes in irradiance, load and dc-link capacitor voltage. The experimental results on a PV based variable dc bus multilevel inverter validate the excellent performance of ASO SHE method in minimizing the total harmonic distortion (THD) and dominant order harmonics under sudden change in operating conditions.

INDEX TERMS Atom search optimization (ASO), multilevel inverter, photovoltaic system, selective harmonic elimination (SHE).

I. INTRODUCTION

Over the past two decades, multilevel inverters (MLIs) have shown their potential in various industrial and renewable energy systems owing to their merits such as modularity, low dv/dt stress, suitability to high power operation, and low THD. It is desirable to improve the efficiency, minimize the size of the inverter, reduce control complexity, and follow strict compliance to harmonics standards such as IEEE 519-2014 and IEC 61000-3-2 to improve the power quality of PV systems [1]. In order to achieve these objectives, SHE control technique is preferred over multicarrier modulation

The associate editor coordinating the review of this manuscript and approving it for publication was Zhehan Yi.

techniques and other non-SHE methods on MLI. Key merits of SHE technique on MLIs are low switching losses, low dv/dt stress on switches and strict control over fundamental and dominant harmonics [2]. Due to its valued merits, SHE technique has drawn the interest of researchers [3]. Despite its various merits, finding the solution to the SHE problem is a complex task. Several numerical methods such as Groebner bases, Walsh function, unified SHE PWM, methods of symmetric polynomial, and optimization techniques exist for solution of SHE problem [4]. The numerical methods provide fast convergence to SHE problem. However, they heavily rely on good estimation of the initial values of the switching angles. In theory of resultants, the degree of polynomial increases as the number of switching angles increases that increases the computational complexity. In Walsh function and unified SHE PWM, computation complexity increases as higher number of switching angles are to be found. To alleviate these problems, researchers have proposed the applications of optimization techniques in solving the SHE problem [5]. In optimization technique, SHE equations are first transformed into a fitness function subjected to switching angle constraint ($0 < \alpha < \pi/2$). Then, fitness function is minimized or maximized by applying a suitable optimization technique. Some of the popular optimization techniques used in solving SHE problem are genetic algorithm (GA), particle swarm optimization (PSO), Imperialistic colonial algorithm (ICA), bee algorithm, colonial competitive algorithm (CCA), firefly, and bacterial foraging algorithm (BFA) etc. In [6], the PSO technique for minimization of harmonics in an 11-level inverter is used. However, PSO often got stuck into the local minima solution, which is undesirable. In [7], bee algorithm to solve the SHE problem for finding the switching angles for 7-level inverter is applied. Though, it achieved higher probability of convergence as compared to GA, it takes large number of iterations. In [8] and [9], the authors applied ICA to find switching angles for 7-level and 11-level inverters. It performed better than CCA, PSO, and GA in terms of harmonics minimization. In [10], firefly algorithm based SHE method, which obtained lower THD value as compared to PSO and BA is proposed. In [11], the authors implemented GA on 7-level switched battery boost MLI. It was shown that GA performed better as compared to sine PWM, however, comparative analysis was not performed against other metaheuristic based SHE methods. In [12], whale optimization algorithm (WOA) based SHE was implemented on an 11-level inverter. However, it has a slower rate of convergence. In [13], the authors proposed a hybrid fish swarm optimization (FSO) SHE, which achieved better fitness as compared to PSO and FSO. In [14], authors proposed a PSO based memetic SHE method for 7-level inverter. It showed a high convergence rate as compared to PSO, GA and BA. Despite their advantages, both of these methods require hybridization of two metaheuristic methods, enhancing the complexity of the algorithm. In [15], the authors implemented TLBO SHE on 5-level CHB MLI. The key feature of this method is its ability to optimize the dc source. However, this method consumes a larger number of iterations, and is practically infeasible to adjust dc sources in the PV system. In [16], researchers implemented hybrid GSA method to solve SHE problem in 9-level inverter. In this method, GSA and PSO run in parallel, requiring more memory space to save a large number of parameters. In the traditional PSO, a particle (bird) uses three distinct behaviors to hunt for the globally best outcome: cognitive, social, and inertial. The foraging action, which helps the flock of birds find food, is made up of cognitive and social behaviors. The anti-predatory behavior of birds is another movement that has been noticed. This makes it easier for the many to flee from predators [17]. From the above discussion, it is clear that there is a need to develop a simple metaheuristic based SHE technique, which can solve SHE equations with less complexity, fast rate of convergence and high accuracy as compared to other metaheuristic based SHE methods.

SHE technique can be applied to conventional MLI topologies with PV systems such as Neutral point clamped (NPC) MLI, flying capacitor (FC) MLI and cascaded H-bridge (CHB) MLI. However, these conventional MLI topologies have demerits such as high component count, losses, control complexity and poor reliability that hinder their application in PV systems. Therefore, researchers focused extensively on reduced component count hybrid MLI topologies in PV systems to gain their topological advantages. Some of the MLI topologies recently used in PV systems are being discussed. In [18], the authors proposed a 9-level inverter topology with voltage boost capability for PV application. Though, this topology reduces the number of switches, it is complex and implemented with high switching frequency. In [19], the authors proposed a 5-level flying capacitor (FC) topology for PV application with 11 switches that requires capacitor voltage balance method. In [20], the authors proposed a modified pack U-cell (PUC) 7-level MLI with asymmetric sources for PV application. The M-dc-link topology proposed in [21] decreases the number of switches by fifty percent as compared to CHB MLI. However, it has a major drawback as it uses high voltage rating switches. In [22], the authors proposed a 25-level inverter topology with 90% efficiency. However, it suffers from asymmetric dc sources, capacitor voltage balancing and bi-directional switches, increasing the cost and the controller complexity. In [23], the authors suggested a PV-based 7-level RS MLI with a DC-DC boost converter to increase the number of output levels with fewer switches, resulting in a multilevel inverter that is smaller, lighter, and less expensive. In [24], the authors improved the power quality of new RCC MLI by using GA and anti-predatory PSO based SHE technique. In [25], the researchers investigated the performance of RCC MLI with MPPT and GA based SHE technique for PV system application. There are some other hybrid topologies implemented in PV systems [26], [27], [28] which claim improvement in efficiency of RES. However, there is lack of study in the available literature which investigates the performance of appropriate SHE method on PV based hybrid MLI topology subjected to sudden change in

operating conditions. Hence, there is a need to implement a SHE method on appropriate hybrid MLI topology for PV application.

The following research gaps have been identified which forms the basis of this work:

•There is a need to develop a simple metaheuristic based SHE technique, which can solve SHE equations with a fast rate of convergence and higher accuracy as compared to existing metaheuristic based SHE methods.

•There is a need to investigate the performance of a suitable metaheuristic based SHE technique on PV based hybrid MLI topology under dynamic change in operating conditions.

Hence, it is desirable to develop a highly accurate metaheuristic based SHE method with fast convergence rate and analyze its performance on hybrid MLI topology for PV application subjected to dynamic change in operating conditions.

Therefore, in this paper to bridge the above discussed research gaps, the authors have proposed the following objectives.

•ASO algorithm to solve SHE problem for a 11-level variable dc bus MLI topology.

•Investigation of the proposed SHE method on PV based hybrid MLI under dynamic change in irradiance, load and dc-link capacitor voltage.

•Real-time implementation of the proposed SHE method on a laboratory scale prototype.

The rest of the manuscript is organized as follows: Section II discusses the mathematical formulation of SHE problem for 11-level MLI. Section III explains the working of proposed ASO based SHE method with its mathematical model. Section IV provides comparative analysis of the proposed SHE method with respect to other state-of-the-art metaheuristics on SHE fitness function. Section V presents the simulation results of the proposed SHE method under sudden change in operating conditions. Section VI elaborates the experimental setup and experimental validation of the simulation results. Finally, section VII concludes the paper and highlights the key findings.

II. SELECTIVE HARMONC ELIMINATION PROBLEM

An 11-level CHB inverter requires five isolated dc sources which may be derived from PV panels. In practical case, the magnitudes of dc sources are generally unequal and can be expressed as in (1).

$$V_{d1} = p_1 V;\ V_{d2} = p_2 V;\ V_{d3} = p_3 V;\\ V_{d4} = p_4 V;\ V_{d5} = p_5 V \tag{1}$$

where, V_{d1}, V_{d2}, V_{d3}, V_{d4}, and V_{d5} represents the dc sources while V is the nominal voltage rating of each dc source. p_1, p_2, p_3, p_4, and p_5 are constant multiplication factors. For equal dc sources; $p_1 = p_2 = p_3 = p_4 = p_5 = 1$.

A typical voltage waveform of an 11-level multilevel inverter is shown in Figure 1. Here, α_1, α_2, α_3, α_4, and α_5 are switching angles, where each angle lies with range

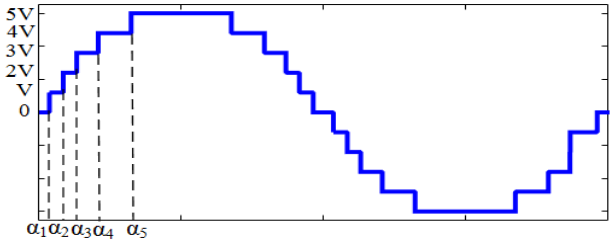

FIGURE 1. 11-level MLI voltage waveform.

$0 \leq \alpha_i \leq \pi/2$ radian. This output voltage waveform consists of fundamental voltage component along with several odd-order harmonics. Since, triplen odd order harmonics are eliminated in line voltage of three-phase inverter, there is need to efficiently control the fundamental and 5th, 7th, 11th and 13th order harmonic voltages. The amplitude of actual fundamental voltage, V_1 is mathematically expressed as in (2).

$$V_1 = \frac{4V}{\pi}[p_1 cos\alpha_1 + p_2 cos\alpha_2 + p_3 cos\alpha_3 \\ + p_4 cos\alpha_4 + p_5 cos\alpha_5] \tag{2}$$

However, desired fundamental voltage, V_1^d depends upon the value of modulation index, M. Relation between M and V_1^d is expressed as in (3).

$$M = \frac{V_1^d \pi}{4 \times (p_1 + p_2 + p_3 + p_4 + p_5) \times V} \tag{3}$$

Amplitude of 5th harmonic, V_5 can be expressed as in (4)

$$V_5 = \frac{4V}{5\pi}[p_1 cos\,(5\alpha_1) + p_2 cos\,(5\alpha_2) + p_3 cos\,(5\alpha_3) \\ + p_4 cos\,(5\alpha_4) + p_5 cos\,(5\alpha_5)] \tag{4}$$

Amplitude of 7th harmonic, V_7 can be expressed as in (5)

$$V_7 = \frac{4V}{7\pi}[p_1 cos\,(7\alpha_1) + p_2 cos\,(7\alpha_2) + p_3 cos\,(7\alpha_3) \\ + p_4 cos\,(7\alpha_4) + p_5 cos\,(7\alpha_5)] \tag{5}$$

Eq. (6) shows amplitude of 11th harmonic, V_{11} while (7) represents amplitude of 13th order harmonics as;

$$V_{11} = \frac{4V}{11\pi}[p_1 cos\,(11\alpha_1) + p_2 cos\,(11\alpha_2) + p_3 cos\,(11\alpha_3) \\ + p_4 cos\,(11\alpha_4) + p_5 cos\,(11\alpha_5)] \tag{6}$$

$$V_{13} = \frac{4V}{13\pi}\left[p_1 \cos\,(13\alpha_1) + p_2 \cos\,(13\alpha_2) + p_3 \cos\,(13\alpha_3) \\ + p_4 \cos\,(13\alpha_4) + p_5 \cos\,(13\alpha_5)\right] \tag{7}$$

In SHE problem for 11-level inverter, it is required to meet the following two conditions simultaneously. The first condition is to keep the amplitude of actual fundamental voltage, V_1 equal to amplitude of desired fundamental voltage, V_1^d for a chosen value of M. The second condition is to eliminate V_5, V_7, V_{11}, and V_{13} by equating eq. (4), (5), (6) and (7) to zero. By solving these equations simultaneously for chosen M, we find firing angles α_1, α_2, α_3, α_4, and α_5. In order to

solve this SHE problem using metaheuristic techniques, it is essential to express it in the form of a fitness function as in (8).

$$f = \min_{\alpha_i} \left\{ \left(100 \frac{(V_1^d - V_1)}{V_1^d} \right)^4 + \frac{1}{4 \times 5} \left(100 \frac{V_5}{V_1} \right)^2 + \frac{1}{4 \times 7} \left(100 \frac{V_7}{V_1} \right)^2 + \frac{1}{4 \times 11} \left(100 \frac{V_{11}}{V_1} \right)^2 + \frac{1}{4 \times 13} \left(100 \frac{V_{13}}{V_1} \right)^2 \right\} \quad (8)$$

where, $0 \leq \alpha_i \leq \frac{\pi}{2}$

In (8), the first term represents the percentage error in the fundamental voltage, which is penalized by power of four. This error shows the difference between its desired and actual values. Other terms represent the percentage amplitude of 5^{th}, 7^{th}, 11^{th}, and 13^{th} harmonics with respect to fundamental voltage harmonic, which is penalized by power two.

III. PROPOSED ATOM SEARCH OPTIMIZATION SHE ALGORITHM

ASO algorithm is a physics-inspired population-based metaheuristic algorithm proposed by Zhao et al. in 2019 [29]. The algorithm motivates from the molecular dynamics and mathematically models the natural atomic motion.

The smallest segment of a chemical compound is a molecule, which is composed of atoms that are held together by covalent bonds. Atoms have complex structures while present in either gas, liquid, or solid form. All atoms in molecules interact with each other and are in a state of constant motion. Since in an atomic system there are millions of atoms, therefore it is difficult to examine the movement and properties of atoms using conventional techniques. Over the years with the development of computer aided technology it has become easier to examine the movement of atoms. In an atomic system physically, there are two interactive forces among atoms i. e. attractive and repulsive forces which cause the movement of atoms. These two forces can be well defined through the potential energy of atoms and in literature there exists many mathematical model which outlines atoms potential energy. Lennard-Jones (L-J) potential is one of the elementary mathematical model that represents the non-constraint interaction forces between atoms while the bond-length potential is another mathematical model that acknowledges constraint forces between atoms. The ASO algorithm considers constraint and non-constraint interaction forces between atoms to model the movement of atoms in molecules.

In ASO algorithm initially, a random population of atoms is initialized in the search space where the position of atoms represents a solution. All atoms have some mass and over the course of iterations, lighter mass atoms move towards the heavier mass atoms through interaction and repulsive forces defined by L-J potential and through bond-length potential caused due to weighted position difference between atoms and best atom. In order to maintain balance between

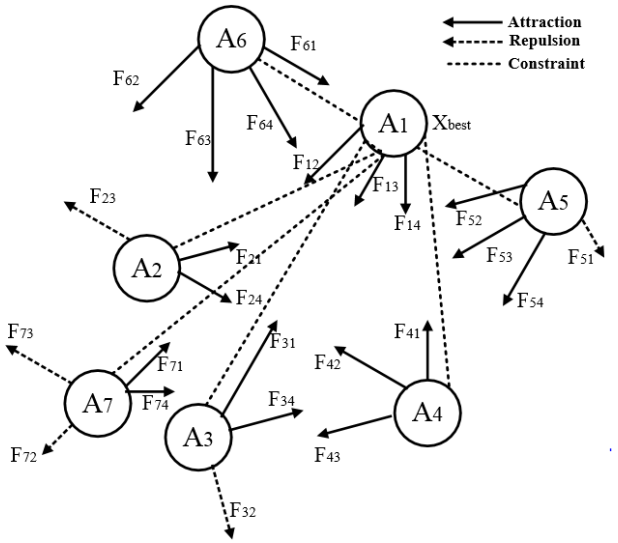

FIGURE 2. Pictorial representation of forces experienced between atoms in ASO algorithm.

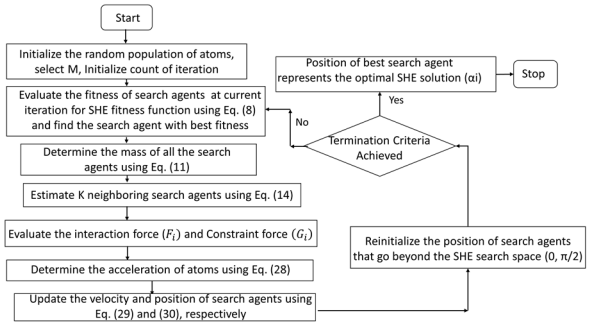

FIGURE 3. Flow chart of ASO method to solve SHE problem.

exploration and exploitation initially atoms interact with all other atoms to better explore the search space and later atoms interact with fewer atoms to attain good exploitation capability. A parameter K maintains this balance and gradually decreases over the lapse of iterations. The pictorial representation of forces experienced between atoms and the flowchart of the ASO algorithm is shown in Figure 2 and Figure 3, respectively.

Table 1 defines the parameters of the ASO algorithm used in solving the SHE problem. The following steps outline the mathematical model of ASO algorithm:

Step 1: Initialize the random population of atoms (search agents) in the search space. Position of i^{th} atom is represented as

$$y_i = \left[y_i^1, \ldots\ldots\ldots\ldots y_i^D \right], \mathrm{i} = 1, \ldots\ldots\ldots\ldots, \mathrm{N} \quad (9)$$

where, y_i^d $(d = 1, \ldots\ldots\ldots\ldots, D)$ signifies the d^{th} component of i^{th} atom in a D-dimensional space. For 11-level inverter, dimension of SHE search space is D=5. Position of each atom, y_i represents the solution of SHE problem. It consists of a set of five switching angles. The boundary of SHE search space is $(0, \pi/2)$ radians.

TABLE 1. Parameters of atom search optimization algorithm.

Parameters	Description
$y_i(t)$	Position of ith atom (search agent) at the tth iteration
$y_{best}(t)$	Position of the best search agent at the tth iteration
N	Number of search agent (Population size) = 30
D	Dimension of the problem = 5
Lower bound	0
Upper bound	$\pi/2$ radians
$m_i(t)$	Represents the ith search agent mass at the tth iteration
$Fit_i(t)$	Fitness of the ith search agent at the tth iteration
$Fit_{best}(t)$	Fitness of the best search agent at the tth iteration
$Fit_{worst}(t)$	Fitness of the worst search agent at the tth iteration
t	Current iteration
T	Maximum number of iterations = 200
K	Number of neighbouring search agent
$F_i^d(t)$	Total interaction forces acted on ith search agent in the dth dimension at tth iteration
$F_{ij}^d(t)$	Interaction force acted on ith search agent from the jth search agent in the dth dimension at tth iteration
$rand_j$	Random number in the interval [0, 1]
$Kbest$	Represents the first K search agent with best fitness value
$F'_{ij}(t)$	A revised version of interaction force acted on ith search agent from the jth search agent at tth iteration
$\sigma(t)$	Represents the length scale which signifies the collision diameter
$\varepsilon(t)$	Represents the depth of the potential well which signifies the interaction strength
$r_{ij}(t)$	Euclidean distance between j^{th} and i^{th} search agent at time t
$\eta(t)$	Depth function
α	Depth Weight = 50
$h_{ij}(t)$	Represents the repulsive or attractive interaction between the ith and the jth search agent
h_{min}	Lower limit of parameter
h_{max}	Upper limit of parameter h = *1.24*
g_o	A constant parameter = 1.1
$g(t)$	Drift factor
$\theta_i^d(t)$	Constraint of the ith atom in the dth dimension at the tth iteration
$G_i^d(t)$	Constraint force acted on the ith search agent in the dth dimension at the tth iteration
$\lambda(t)$	Lagrangian multiplier
β	Multiplier Weight = 0.2
$b_{i,best}$	Fixed bond length between the ith search agent and the best search agent
$a_i^d(t)$	Acceleration of ith search agents in dth dimension and at tth iteration
$v_i^d(t)$	Velocity of ith search agent in the dth dimension at tth iteration
$v_i^d(t+1)$	Velocity of ith search agent in the dth dimension at (t+1)th iteration
$y_i^d(t+1)$	Position of ith search agent in dth dimension at $(t+1)^{th}$ iteration

Step 2: Evaluate the fitness of all the search agents using SHE fitness function in Eq. (8) and find the agent with smallest fitness (for minimization problem).

Step 3: Determine the mass of all the search agents using following equations:

$$M_i(t) = exp^{\frac{Fit_i(t) - Fit_{best}(t)}{Fit_{worst}(t) - Fit_{best}(t)}} \tag{10}$$

$$m_i(t) = \frac{M_i(t)}{\sum_{j=1}^{N} M_j(t)} \tag{11}$$

where, $m_i(t)$ represents the ith search agent mass at the tth iteration, $Fit_{best}(t)$ and $Fit_{worst}(t)$ is the fitness of the agents with best and the worst fitness value at the tth iteration and are defined as:

$$Fit_{best}(t) = \min_{i\in\{1,2,\ldots\ldots,N\}} Fit_i(t) \tag{12}$$

$$Fit_{worst}(t) = \min_{i\in\{1,2,\ldots\ldots,N\}} Fit_i(t) \tag{13}$$

where, $Fit_i(t)$ is the fitness of the ith agent at the tth iteration.

Step 4: Estimate K neighboring search agents using the equation:

$$K(t) = N - \left\{(N-2) * \sqrt{\frac{t}{T}}\right\} \tag{14}$$

where, N is the total number of search agents, t is the current iteration and T is the maximum number of iterations.

Step 5: Evaluate the sum of interaction forces (F_i) acted on ith search agent from other search agents in dth dimension as:

$$F_i^d(t) = \sum\nolimits_{j\varepsilon Kbest} rand_j F_{ij}^d(t) \tag{15}$$

where, $rand_j$ represents the random number in the range [0, 1].

$$F_{ij}(t) = \frac{24\varepsilon(t)}{\sigma(t)}\left[2\left(\frac{\sigma(t)}{r_{ij}(t)}\right)^{13} - \left(\frac{\sigma(t)}{r_{ij}(t)}\right)^{7}\right]\frac{r_{ij}(t)}{r_{ij}^d(t)} \tag{16}$$

$$F'_{ij}(t) = \frac{24\varepsilon(t)}{\sigma(t)}\left[2\left(\frac{\sigma(t)}{r_{ij}(t)}\right)^{13} - \left(\frac{\sigma(t)}{r_{ij}(t)}\right)^{7}\right] \tag{17}$$

where, σ is the length scale which signifies the collision diameter, ε is the depth of the potential well which signifies the interaction strength. $r_{ij}(t)$ is the Euclidean distance between j^{th} and i^{th} atom at t^{th} iteration. A revised version of interactive force is developed which is defined as:

$$F'_{ij}(t) = -\eta(t)\left[2\left(h_{ij}(t)\right)^{13} - \left(h_{ij}(t)\right)^{7}\right] \tag{18}$$

where, $\eta(t)$ denotes the depth function implemented for repositioning the repulsion or attraction region and is defined as:

$$\eta(t) = \alpha\left(1 - \frac{t-1}{T}\right)^{3} e^{\frac{-20t}{T}} \tag{19}$$

α represents the depth weight and $h_{ij}(t)$ is defined in the following manner:

$$h_{ij}(t) = \begin{cases} h_{min}, \frac{r_{ij}(t)}{\sigma(t)} < h_{min} \\ \frac{r_{ij}(t)}{\sigma(t)}, h_{min} \le \frac{r_{ij}(t)}{\sigma(t)} \le h_{max} \\ h_{max}, \frac{r_{ij}(t)}{\sigma(t)} > h_{max} \end{cases} \tag{20}$$

where, h_{min} and h_{max} represents the upper and the lower bound of h and $\sigma(t)$ is represented as:

$$\sigma(t) = \left\| y_{ij}(t), \frac{\sum_{j\in Kbest} y_{ij}(t)}{K(t)} \right\|_2 \tag{21}$$

where, *Kbest* represents search agents with best fitness value.

$$\begin{cases} h_{min} = g_0 + g(t) \\ h_{max=u} \end{cases} \tag{22}$$

where, g represents the drift factor which maintains balance between exploration and exploitation and is defined as:

$$g(t) = 0.1 * sin\left(\frac{\pi}{2} * \frac{t}{T}\right) \tag{23}$$

Step 6: Evaluate the constraint force G_i using the following equations:

$$G_i^d(t) = -\lambda(t)\nabla\theta_i^d(t) \tag{24}$$

where, $\lambda(t)$ represents the Lagrangian multiplier and is defined as:

$$\lambda(t) = \beta e^{-\frac{20t}{T}} \tag{25}$$

where, β denotes the multiplier weights. θ_i is the constraint of the ith atom and is defined as:

$$\theta_i(t) = \left[|y_i(t) - y_{best}(t)|^2 - b_{i,best}^2\right] \tag{26}$$

where, $y_{best}(t)$ represents the position of best search agent at tth iteration, $b_{i,best}$ is fixed bond length between best search agent and ith search agent. Using eq. (26) in eq. (24), and substituting $2\lambda \to \lambda$, constraint force is redefined as:

$$G_i^d(t) = \lambda(t)\left(y_{best}^d(t) - y_i^d(t)\right) \tag{27}$$

Step 7: Determine the acceleration of ith search agents in dth dimension at tth time using constraint and interaction force as follows:

$$a_i^d(t) = \frac{F_i^d(t)}{m_i^d(t)} + \frac{G_i^d(t)}{m_i^d(t)} \tag{28}$$

$$= -\alpha\left(1 - \frac{t-1}{T}\right)^{3} e^{-\frac{20t}{T}} \sum_{j\in Kbest} \frac{rand_j\left[2 * \left(h_{ij}(t)\right)^{13} - \left(h_{ij}\right)^{7}\right]}{m_i(t)} \frac{\left(y_j^d(t) - y_i^d(t)\right)}{\left\|y_i(t), y_j(t)\right\|_2} + \beta e^{-\frac{20t}{T}} \frac{y_{best}^d(t) - y_i^d(t)}{m_i(t)} \tag{29}$$

Step 8: Update the velocity of search agent using following equation:

$$v_i^d(t+1) = rand_i^d v_i^d(t) + a_i^d(t) \tag{30}$$

where, $v_i^d(t+1)$ is the velocity of ith search agent in the dth dimension at (t+1)th iteration and $v_i^d(t)$ is the velocity of ith search agent in the dth dimension at tth iteration.

Step 9: Update the position of ith search agent in dth dimension using equation (31)

$$y_i^d(t+1) = y_i^d(t) + v_i^d(t+1) \tag{31}$$

Step 10: Determine the search agent that goes beyond the search space of SHE problem and reinitialize their positions.

Step 11: Go to step 2 until the termination criteria is satisfied. It may be the number of maximum iterations or threshold value of SHE fitness function.

Step 12: The position of best search agent represents the global optimal solution.

The next subsections discuss the execution time and computational complexity of the proposed SHE method.

A. ASO EXECUTION TIME

ASO SHE code was run for different values of modulation indices in MATLAB/Simulink environment. Table 2 shows the execution time taken by the ASO SHE method for 100, 200, and 500 iterations, respectively. It was found that the ASO SHE method required the maximum execution time of 1.4s at iteration = 100. Moreover, the proposed SHE method consumes maximum execution time of 2.15s and 4.82s at 200 and 500 numbers of iterations, respectively.

B. COMPUTATION COMPLEXITY

The computation complexity of the ASO algorithm mainly depends on three processes which include initialization of population, evaluation of fitness function and updation of position of atoms in the search space.

The computation complexity of the initialization process is O(N) while the complexity of updation process is $O(N \times T) + O(K \times T \times D)$ therefore the total computational complexity of the algorithm can be defined as:

$$O(ASO) = O(N \times T) + O(K \times T \times D) \tag{32}$$

TABLE 2. Execution time of the proposed SHE method under different modulation indices.

M	Execution Time at Iter = 100	Execution Time at Iter = 200	Execution Time at Iter = 500
0.8	1.391 s	2.151 s	4.253 s
0.845	1.407 s	2.117 s	4.823 s
0.75	1.359 s	2.103 s	4.256 s
0.7	1.389 s	2.107 s	4.323 s
0.65	1.387 s	2.144 s	4.277 s
0.6	1.371 s	2.142 s	4.264 s
0.55	1.393 s	2.137 s	4.271 s
0.5	1.387 s	2.105 s	4.213 s
0.45	1.368 s	2.114 s	4.233 s

where, N represents the number of search agents, D represents the dimension of the problem, T represents the maximum number of iterations and K represents the number of neighboring search agents.

IV. COMPARATIVE STUDY OF ASO SHE METHOD WITH RECENT METAHEURISTICS

As previously mentioned, various optimization techniques are present in the literature to solve the SHE problem. The authors have carefully selected some of the state-of-the-art optimization techniques to compare the performance of the proposed SHE method. These SHE methods have been discussed along with their shortcomings in the introduction section.

The performance evaluation of proposed ASO algorithm and five other metaheuristics such as TLBO [15], firefly [10], PSO, bee algorithm [7] and ICA [9] is carried out to solve SHE fitness function. In this case study, the algorithms are applied in solving the SHE problem for the 11-L RCC MLI. Figure 4(a) shows the comparison between the various SHE techniques on the basis of ability to reach optimum fitness value, which is the key performance index (PI). It is evident that the proposed ASO algorithm reaches the fitness ($<10^{-20}$) over wide range of M for the 11-L inverter. The superiority of ASO algorithm over other metaheuristics signifies increased accuracy in the obtained solution for solving the SHE problem. Another important PI is the cumulative distribution function (CDF), which corresponds to the probability of reaching fitness below a reference value (reference = 10^{-15}). The proposed algorithm achieves the highest value of CDF for the 11-L inverter that is just above 40% as shown in Figure 4(b). The CDF values for other metaheuristics were found below 20%. This indicates that the proposed algorithm is more efficient in finding the optimum solution over wide range of M as compared to its counterparts. Based on the above discussion, the efficacy of ASO algorithm is proved in SHE problem. Figure 4(c) exhibits the plot of switching angles versus M for the 11-L inverter. It is interesting to note that for some values of M, multiple solutions are found. The switching angles are computed for M = 0.845, 0.8 and 0.7, respectively using ASO SHE algorithm as shown in Table 3. With the help of switching angles shown in Figure 4(c), the harmonic content and THD values in the line voltage of the 11-L inverter have been computed and plotted with respect to M as shown in Figure 4(d). It is found that the line voltage THD is below 5% as per the IEEE std. 2022 [30]. Figure 4(e) and Figure 4(f) effectively demonstrate the mitigation of dominant harmonics under wide range of M in linear and semilog scale, respectively. It is clear that the magnitude of individual harmonic is well below 5% which is in accordance with the IEEE std 2022. Also, it is found that the average value of the individual (5^{th}, 7^{th}, 11^{th} and 13^{th}) harmonics is around 0.001% due to the excellent performance of the proposed SHE method.

Moreover, Table 4 shows a detailed comparison between the proposed and state-of-the-art SHE method for M = 0.8. The results exhibit that ASO SHE method provided lowest line voltage THD (in percentage) as well as lowest percentage values of error in fundamental voltage (h_{1e}) as compared to other SHE methods. The proposed SHE method also achieved lowest percentage values of 5^{th} harmonic voltage (h_5), 7^{th} harmonic voltage (h_7), 11^{th} harmonic voltage (h_{11}), and 13^{th} harmonic voltage (h_{13}) as compared to PSO, Bee, TLBO, ICA and firefly SHE methods. The lowest values of these parameters (fitness value, THD, h_{1e}, h_5, h_7, h_{11} and h_{13}) indicate that ASO SHE method provides superior SHE solution as compared to other methods.

To ensure fairness of the comparison between the proposed and other SHE methods, two key performance parameters were chosen. One of the main parameters is quality of the SHE solution obtained. This parameter is expressed in terms of accuracy of SHE fitness value. The lowest value of SHE fitness value is desirable as it corresponds to a superior SHE solution. It can be seen from Table 4 that the proposed ASO SHE method holds the lowest SHE fitness value. Therefore, it results in minimum percentage error in the fundamental voltage as well as the lowest percentage values of 5^{th}, 7^{th}, 11^{th}, and 13^{th} harmonics as compared to other SHE methods. Another performance index for comparison is rate of convergence of SHE methods to reach optimal value. ASO SHE method has the fastest rate of convergence as compared to other SHE methods as it reaches the optimum SHE fitness within same number of iterations.

V. PERFORMANCE ANALYSIS OF PROPOSED SHE METHOD ON A STAND-ALONE PV SYSTEM

The proposed ASO SHE method is applied on an 11-level variable dc bus MLI topology which is a RCC topology. In [16], the authors proposed the 9-level configuration of this RCC topology. It is desirable to implement the proposed SHE method on RCC MLI as it provides benefits of SHE and RCC MLI together. The variable dc bus MLI topology is derived from the hybridization of multilevel dc link inverter [31] and modified H-bridge cascaded inverter [32]. The key features of this topology are reduction in total count of switches and drivers, high modularity, low conduction loss, use of unidirectional switches, no requirement of capacitors and diodes, and use of two variable dc buses. The working principle and

TABLE 3. Computed switching angles using ASO SHE method.

M	Fitness value	α_1 (rad.)	α_2 (rad.)	α_3 (rad.)	α_4 (rad.)	α_5 (rad.)
0.845	$1.6\text{x}10^{-13}$	0.14625	0.21835	0.42047	0.62689	1.00375
0.8	$1.5\text{x}10^{-11}$	0.1147	0.33057	0.4745	0.78784	1.08637
0.7	$4.9\text{x}10^{-13}$	0.1438	0.50016	0.7209	0.9327	1.2808

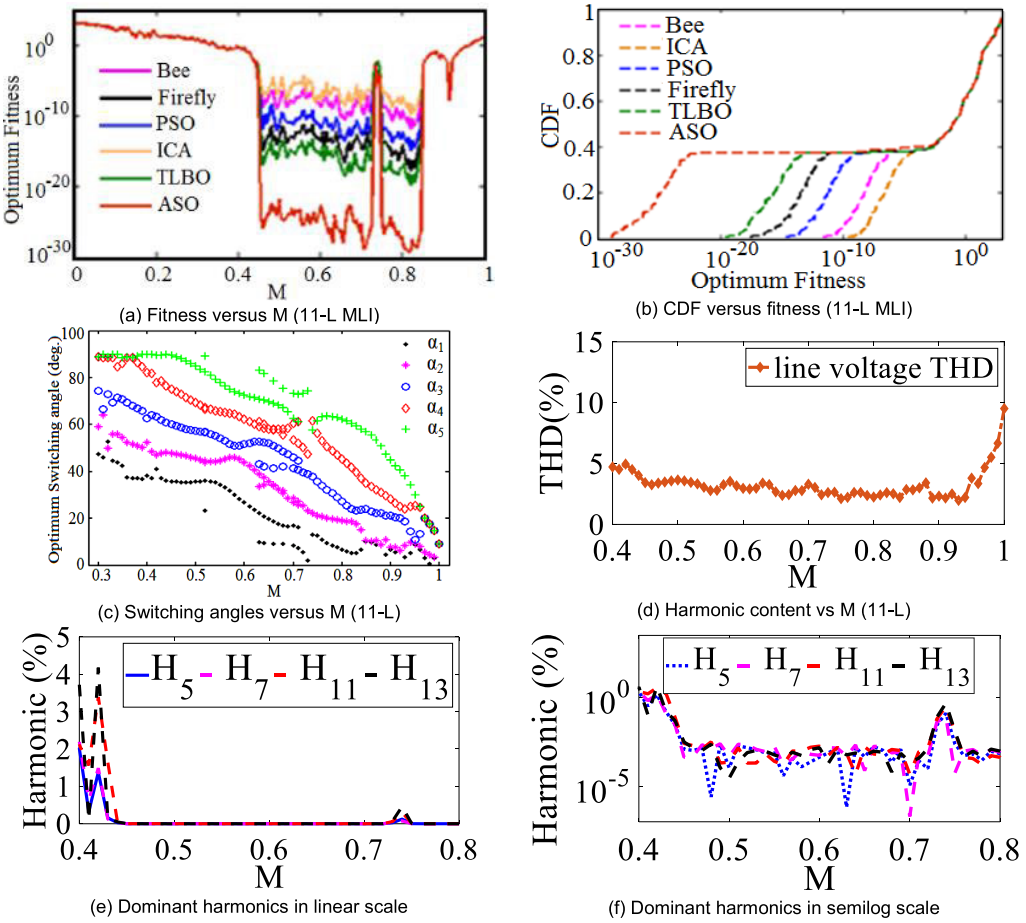

FIGURE 4. Performance of ASO in SHE problem.

TABLE 4. Comparison of harmonic profile for M=0.8.

SHE	Fitness value	THD_{line} (%)	Harmonic Level (% of fundamental)				
			h_{1e}	h_5	h_7	h_{11}	h_{13}
ASO	$1.5\text{x}10^{-11}$	4.5	0.003	$3.8\text{x}10^{-7}$	$6.7\text{x}10^{-7}$	$1.1\text{x}10^{-6}$	$8\text{x}10^{-7}$
PSO	$1.5\text{x}10^{-4}$	5.2	0.14	0.02	0.16	0.03	0.13
Bee	$1.5\text{x}10^{-2}$	5.9	0.28	0.37	0.4	0.25	0.32
TLBO	$1.8\text{x}10^{-2}$	6.1	0.31	0.38	0.43	0.28	0.3
GSA	$1.5\text{x}10^{-3}$	5.45	0.2	0.08	0.24	0.1	0.2
Firefly	$2.8\text{x}10^{-2}$	6.2	0.26	0.4	0.3	0.32	0.25

switching strategy of this RCC topology is given in [16].To further evaluate the benefits of the 11-L hybrid MLI topology a comparison is carried out with other recently developed MLI topologies as in Table 5.

The comparison is carried out based on quantitative parameters such as Number of dc sources (Nsource), Number of switches (Nswitch), Number of components (Ncomp), Number of capacitors (Ncap), and Number of diodes (Nd). Additionally, comparison is also carried out among the 11-level MLI topologies based on few qualitative parameters such as requirement of charge balancing circuit and scheme, symmetric/asymmetric, and the modulation scheme used. From

TABLE 5. Comparison between the recently published 11-level MLI topologies.

Topology used	Nsource	Nswitch	Ncomp	Ncap	Nd	Charge balance circuit and scheme	Symmetric	Technique used
11-level Hybrid MLI	5	12	17	0	0	Not required	yes	ASO SHE
11-level SDDS MLI [28]	8	8	20	0	4	Not required	yes	modified fish swarm optimization
WE-type 11-level Inverter [33]	1	11	14	2	0	required	No	Differential Evolution SHE
UXE type 11-level inverter [34]	1	12	22	2	7	required	No	Hybrid PWM
Boost ANPC 11-level Inverter [35]	1	12	17	4	0	required	No	level-shifted SPWM
11-level HC MLI [36]	2	12	15	1	0	required	No	MGWO

the comparison, it can be seen that the 11-level hybrid MLI topology used in this work and 11-level SDDS MLI [28] are symmetric and multisource topologies that do not require charge balance circuit and scheme. On the contrary, WE-type 11-level Inverter [33], UXE type 11-level inverter [34] and boost ANPC 11-level Inverter [35] are asymmetric and single source topologies which require charge balance circuit and scheme due to the presence of capacitors. In terms of quantitative comparison with 11-level SDDS MLI topology, the 11-level hybrid MLI topology excels in terms of N_{source}, N_d and N_{comp}. On comparison with single-source UXE type 11-level MLI [34] and boost ANPC 11-level Inverter [35], it is found that the hybrid MLI topology requires lesser number of components (Ncomp) as compared to [28] while it has same Ncomp as required in boost ANPC 11-level Inverter [35]. It can be observed from the comparison that 11-level MLI topologies proposed in [34] and [36] hold lower value of Ncomp as compared to 11-level hybrid MLI topology. However, these topologies [34] and [36] require the use of asymmetric dc sources and complex charge balance circuit and scheme.

In the following sub-section, ASO SHE method is implemented and analyzed in this RCC MLI topology with PV system.

A. PERFORMANCE OF PROPOSED SHE METHOD UNDER DYNAMIC CHANGE IN OPERATING CONDITIONS

The proposed hybrid SHEPWM is tested on a 1.6 kW stand-alone PV-based battery energy storage system (BESS) to validate the performance in MATLAB/Simulink environment as shown in Figure 5. The stand-alone PV system consists of five PV modules whose parameters are given in Table 6 and are connected to five batteries via bi-directional dc/dc converter. The five independent batteries are used to efficiently regulate the five dc-link capacitor voltages under dynamic change in irradiance and load conditions. The dc/dc boost converter is controlled using a suitable MPPT algorithm to extract maximum power under sudden change in irradiance and load [37]. Three case studies have been carried out to evaluate the performance of the proposed SHE method on a stand-alone PV system under sudden change in operating

TABLE 6. Parameters of stand-alone PV with BESS.

N	P_{mpp} (W)	V_{mpp} (V)	I_{mpp} (A)	V_{oc} (V)	I_{sc} (A)	β_{oc} (%/^{0}C)	α_{sc} (%/^{0}C)	Cap.
72	325	37.5	8.67	45.8	9.42	-0.31	0.0402	80Ah

TABLE 7. Simulation parameters.

Atoms (Search Agents)	Maximum iteration	Dimension	Alpha (α)	Beta (β)	h_{max}	g_0
30	200	5	50	18	1.24	1.1

conditions. In the first case study, the proposed method is tested under sudden variation in irradiance. The second case study investigates the behavior of the system under simultaneous sudden change in irradiance and load. The final case study evaluates the performance of the proposed method during sudden change in the magnitude of the dc-link capacitors voltage. The simulation parameters are listed in Table 7.

Case study 1: Under sudden change in irradiance

In this case study, the performance of the proposed SHE method is evaluated on a stand-alone PV system under dynamic sudden change in irradiance. For this case, the PV system is operated at a starting irradiance of G = 500W/m^2. After some time, at t = 0.3s the irradiance is instantly increased to G = 1000W/m^2. The system is tested on a constant RL load with R = 10Ω and L = 200mH. The zoomed responses of the PV module power and dc-link capacitor voltage are shown in Figure 6(a) – (b) respectively. The meticulously designed dc-link voltage control maintains a constant voltage of 12V at the dc-link capacitor under varying irradiance conditions. Owing to this excellent control, load voltage and load current waveforms do not show significant difference during varying irradiance condition as shown in Figure 6(c)–(d), respectively. It can be seen that the load voltage waveform has 11 output levels while load current approximates sine waveform due to behavior of inductive load as a filter. The harmonic distribution plot of load voltage during sudden change in irradiance G = 500W/m^2 is shown in Figure 6(c). It is evident that during the sudden change in irradiance the fundamental peak voltage is 64.38 V and phase

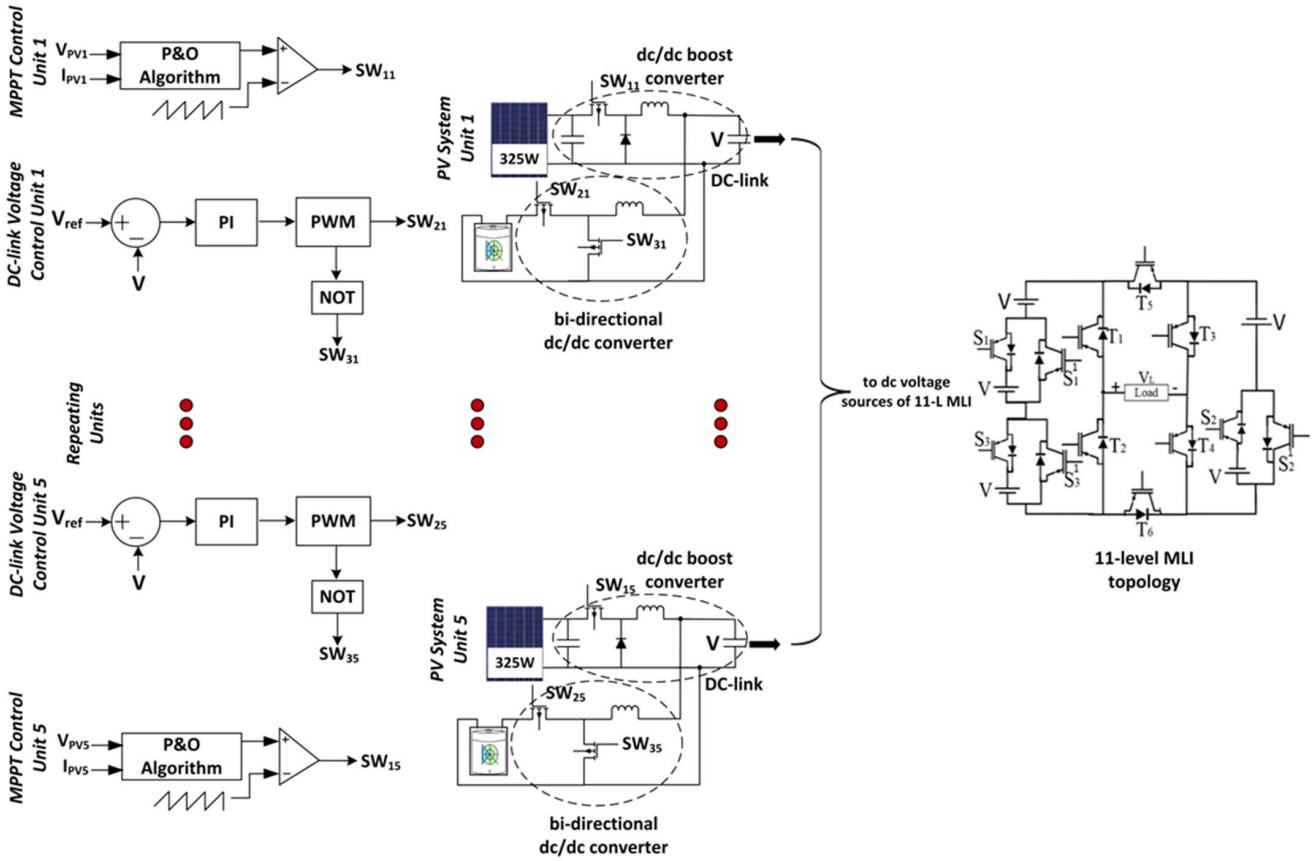

FIGURE 5. 11-Level MLI with proposed method for stand-alone PV with BESS.

THD is around 7.58 % which is nearly equal to the value of fundamental peak voltage and THD just before the change in the irradiance. It is also shown that 5th, 7th, 11th and 13th order harmonics were minimized effectively by the proposed ASO based SHE method during the sudden change in irradiance.

Case study 2: Under simultaneous sudden change in irradiance and load

In the second case, the proposed SHE method is tested under simultaneous sudden change in irradiance and load. The system is initiated with a starting irradiance of G = 1000W/m^2 for a RL load with R = 10Ω and L = 200mH. After some time at t = 0.3s, the irradiance and load impedance are instantly reduced to G = 500W/m^2 with R = 5Ω and L = 100mH. The zoomed response curves of the power extracted from the PV module, dc-link capacitor voltage, load voltage and current waveforms are shown in Figure 7(a) – (d). Fig. 7(a) shows the reduction in power from the PV module at 0.3s. The dc-link voltage control loop helps in efficiently regulating the dc-link capacitor voltage as shown in Figure 7(b). Due to the fine voltage regulation of the dc-link controller, load voltage waveform shows no significant variation after t = 0.3s. Moreover, the load current quickly settles down to the new steady-state value as shown in Figure 7(d). The increase in the value of the current is due to the reduction in the load. Figure 7(c) shows the harmonic profile of load voltage under simultaneous sudden variation in irradiance and load. It can be easily observed that the THD level and 5th, 7th, 11th and 13th harmonics are effectively minimized by the proposed ASO SHE technique during simultaneous sudden variation of irradiance and load. The THD value of phase voltage and fundamental peak voltage is around 7.53% and 64.14 V, respectively, which is almost equal to the THD value of phase voltage and fundamental peak voltage before the simultaneous variation in irradiance and load.

Case Study 3: *Under sudden change in the dc-link capacitor voltage*

In the final case study, the proposed ASO algorithm is tested during sudden change in the magnitude of the dc-link capacitors voltage. To investigate the performance of the proposed SHE method under sudden change in the magnitude of the dc-link capacitors voltage, the reference values of the dc-link capacitor is changed from 12V to 24V at t = 0.2s as shown in Figure 8(a). The PV modules are operated at STC whereas the 11-L MLI is connected to a constant RL load with R=10Ω and L=200mH. The zoomed response curves of the dc-link capacitor voltage, load voltage and current waveforms are shown in Figure 8(a) – (d). The voltage across the dc-link capacitor quickly settles to the new reference value of 24 V as shown in Figure 8(b) at 0.2s. Similarly, the dc-link capacitor

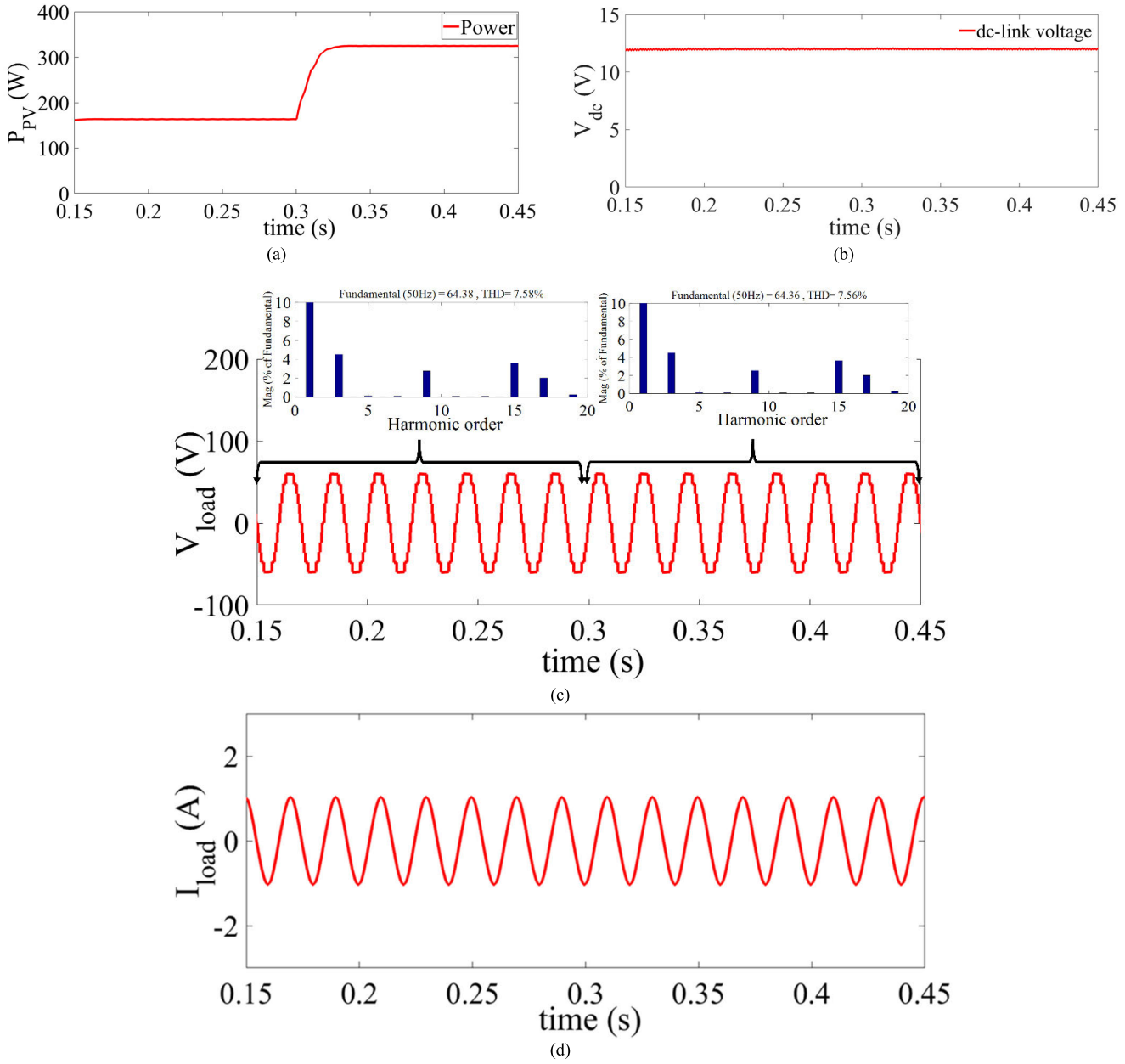

FIGURE 6. Zoomed responses of (a) PV power, (b) dc-link capacitor voltage, (c) load voltage and (d) load current along with their harmonic plots under dynamic sudden change in irradiance.

reaches the new target value of 12 V from 24 V at 0.4s. These results indicate that the dc-link voltage quickly settles down to the new reference value and ensures stability of the stand-alone PV system.

The load voltage and current waveforms follow the dc-link reference voltage as shown in Figure 8(c)–(d), respectively. The harmonic plot of load voltage indicates a THD of 7.48% and fundamental peak voltage 64.32V between t = 0.15s to 0.2s. For t = 0.2s to t = 0.4s, the THD of phase voltage is 7.43% while the fundamental peak voltage is 128.8 V which is equal to the desired values as the new dc-link capacitor voltage is 24 V during t = 0.2s to t = 0.4s. After t = 0.4s, the voltage waveform has a THD of 7.49% and the fundamental peak voltage is 64.32 V as dc-link capacitor voltage decreases to 12 V as shown in Figure 8(c). It is clear that the 5^{th}, 7^{th}, 11^{th} and 13^{th} harmonics are effectively suppressed by using the proposed ASO SHE method during sudden change in dc-link capacitor voltage.

It is interesting to note that for 11-level multilevel inverter, a five dimensional SHE technique is used to compute the switching angles which can control five harmonics as degree of freedom is five. One of them is the fundamental harmonic while others are 5^{th}, 7^{th}, 11^{th}, and 13^{th}. Since, balanced three-phase system is generally used in the industrial

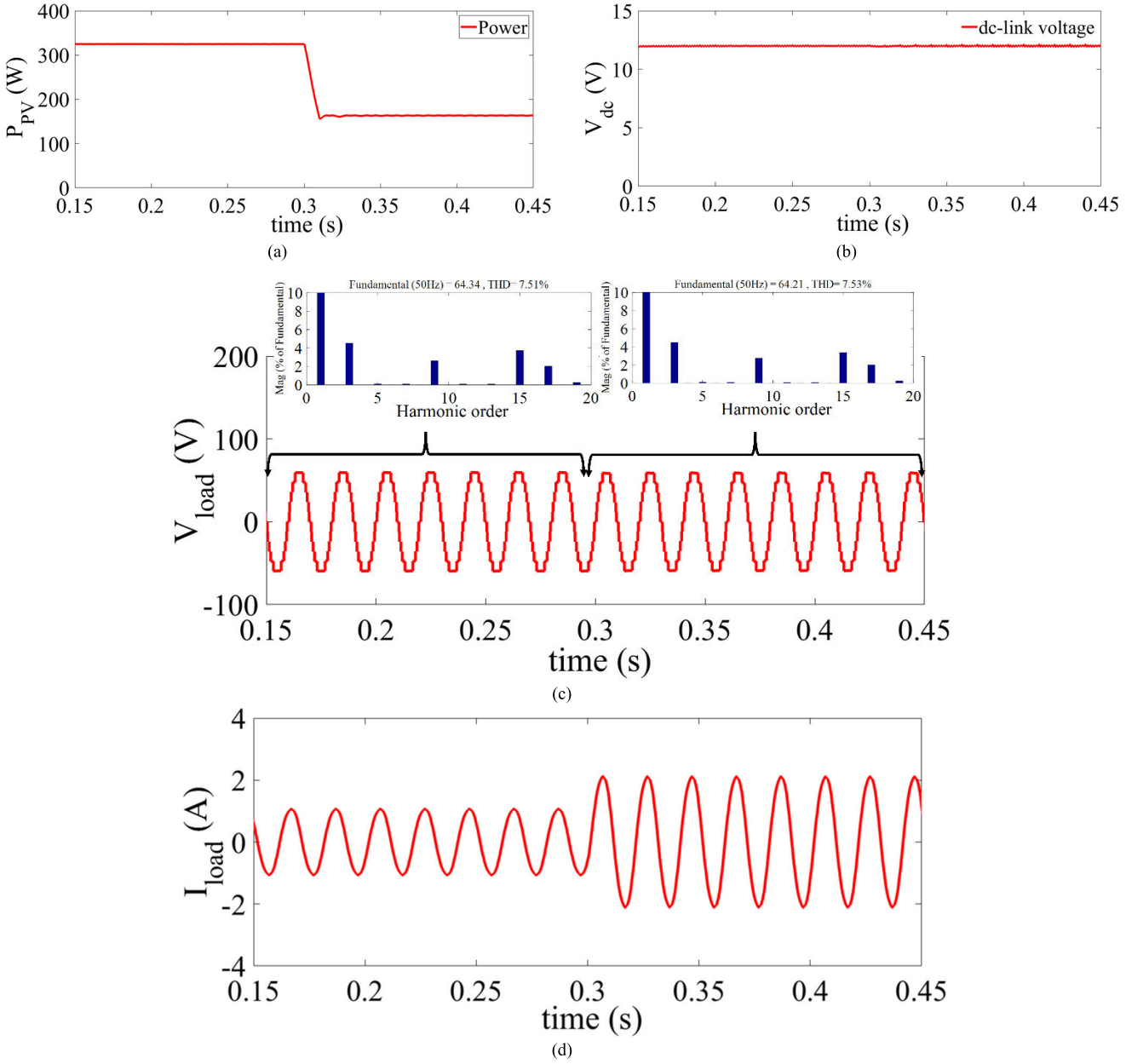

FIGURE 7. Zoomed responses of (a) PV power, (b) dc-link capacitor voltage, (c) load voltage and (d) load current along with their harmonic plots under simultaneous sudden changes in irradiance and load.

applications, dominant triplen harmonics such as 3rd and 9th do not appear in the line-to-line voltage waveform of balanced three-phase 11-level inverter. Therefore, it is not required to eliminate the 3rd harmonic and other triplen harmonics in the SHE technique [3].

VI. EXPERIMENTAL ANALYSIS OF PROPOSED SHE METHOD

To validate the performance of proposed ASO SHE method for enhanced power quality of hybrid MLI based PV system, an experimental setup was developed. Figure 9(a) shows a rooftop solar PV array of 1.6 kW. Figure 9(b) shows the MPPT based charge controllers with battery bank which receive input dc power from rooftop solar PV. The output terminals of these batteries are connected to input dc terminals of developed 11-level inverter. Figure 9(c) shows the 11-level variable dc bus MLI assembly with digital storage oscilloscope (DSO) TDS2024C, power quality analyzer and load bank. There are five input dc terminals which receive 12V dc supply from MPPT controlled isolated batteries (rating 80Ah). There are 12 switching devices (IRFP460) with isolated drivers (FOD3180) as shown in MLI assembly. Figure 10 shows the working mechanism of the proposed SHE method. It shows that the proposed method minimizes

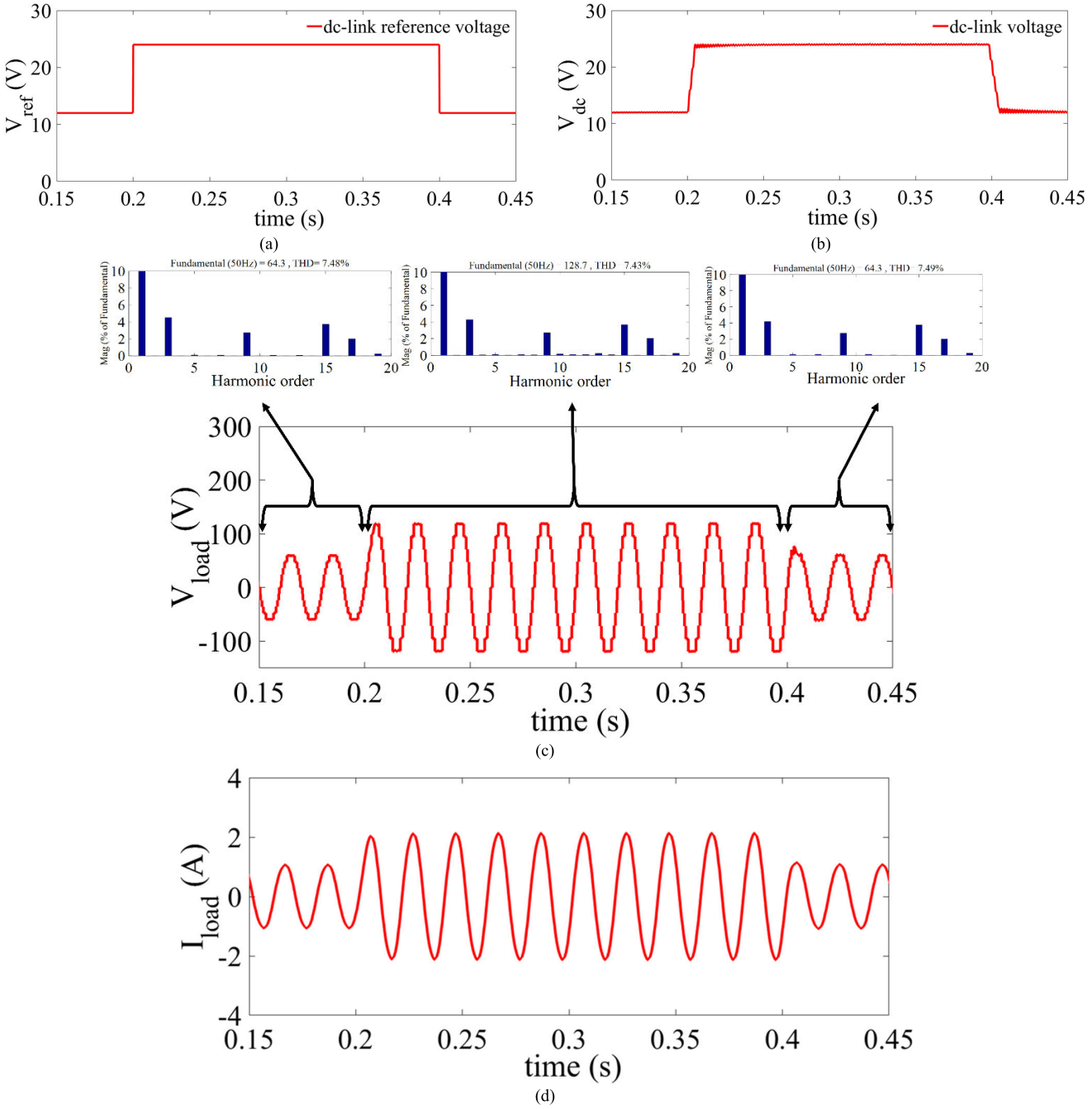

FIGURE 8. Zoomed responses of (a) PV power, (b) dc-link capacitor voltage, (c) load voltage and (d) load current along with their harmonic plots under sudden changes in the reference value of the dc-link capacitor voltage.

the five-dimensional SHE problem for chosen value of M and finds the optimum five switching angles in offline mode. Now, these angles for wide range of M are stored in a lookup table. Figure 11 shows the offline implementation of proposed SHE method on MLI. For a chosen value of M, five switching angles are extracted from the lookup table.

These switching angles are fed to a switching pattern table which is constructed for a complete electrical cycle. Now, a software program is written in embedded C which is used to program the 8-bit microcontroller which generates switching pulses for gate drivers. The gate switching signals are fed to MOSFETs of MLI.

To implement the proposed SHE method in real-time the stored switching angles for chosen values of M are fetched to the switching control algorithm made in the MATLAB /Simulink platform. This switching control algorithm with lookup table will be downloaded on real-time controller. The

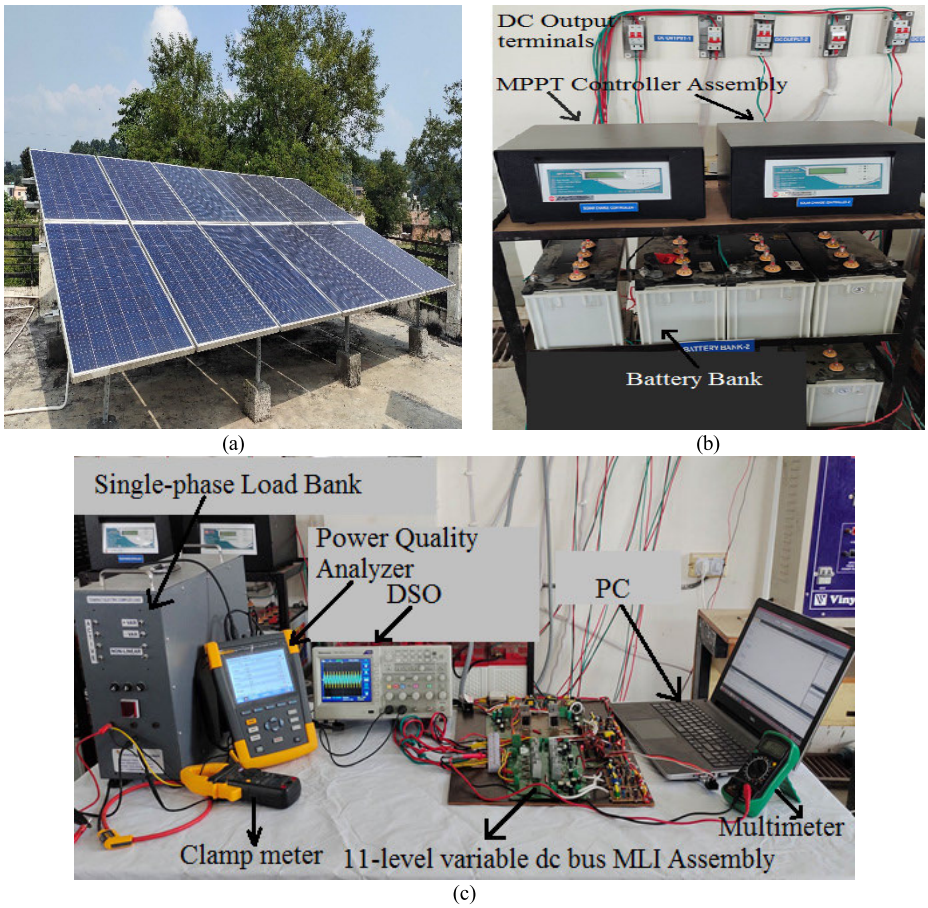

FIGURE 9. Experimental setup of 11-level inverter with PV system: (a) Rooftop PV array of 1.6 kW, (b) MPPT controllers with batteries, (c) Experimental setup of 11-level MLI with load bank.

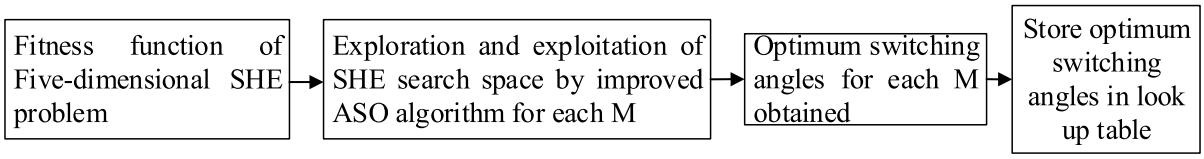

FIGURE 10. Offline switching angle computation using improve ASO.

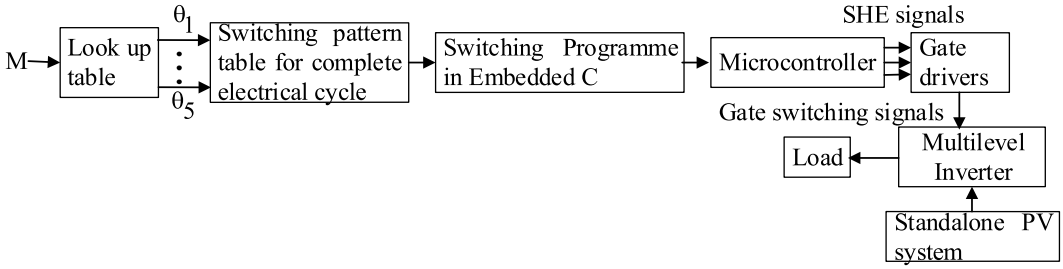

FIGURE 11. Implementation of ASO SHE on MLI.

real-time controller generates the switching pulses for the twelve switches of hybrid MLI according to the desired value of M and thus, the desired value of output voltage. These pulses are extracted from the digital I/O ports of controller to the Gate driver ICs which will turn ON and OFF the MOSFETs [38].

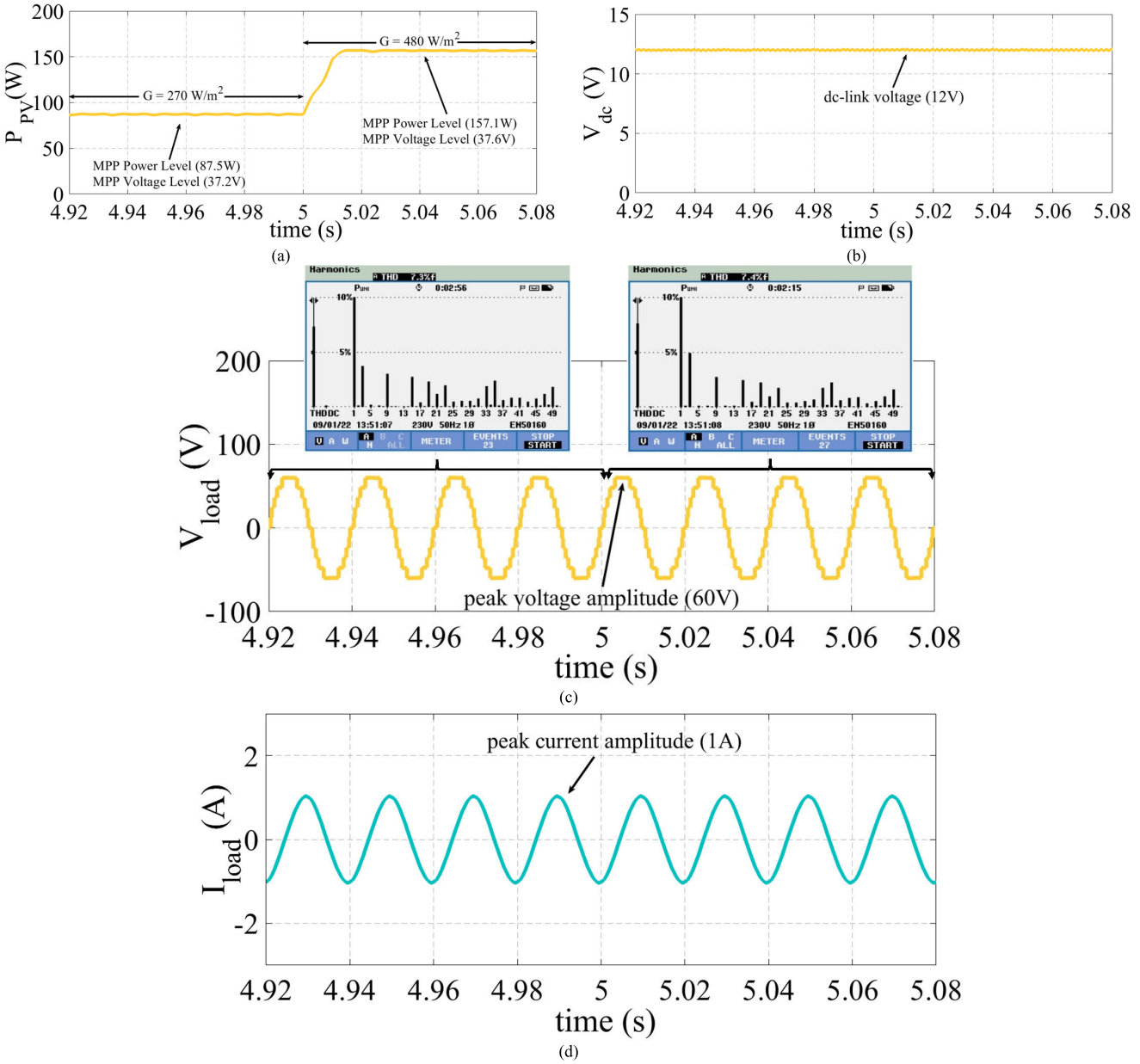

FIGURE 12. Zoomed Experimental waveforms of (a) PV module power, (b) dc-link capacitor voltage, (c) output voltage with its harmonic plot and (e) output current under sudden change in irradiance.

A. EXPERIMENTAL VALIDATION OF THE PROPOSED SHE METHOD UNDER DYNAMIC CHANGE IN OPERATING CONDITIONS

The performance of the proposed SHE method is carried out on three experimental case studies similar to the simulation case studies for hardware validation. DSO is used to store the waveforms in.csv format. The.csv files are then read in MATLAB/Simulink environment for enhanced readability under dynamic change in operating conditions. Since there are five identical dc-link voltage capacitors which are the input sources for the 11-level MLI topology, the power response of one PV module and voltage response of one dc-link capacitor voltage is shown in the experimental case studies.

Case Study 1: Under sudden change in irradiance

In this experimental study, the performance of the proposed SHE method is tested on 11-level multilevel inverter operated at M = 0.75 for a standalone PV system under sudden change in irradiance. The dc-link capacitor reference voltage is chosen as 12V and the 11-L MLI is connected to a constant load of R = 10Ω and L = 200mH. The PV modules are operated with a starting irradiance of G = 270W/m^2. After some time, at t = 5s the irradiance is suddenly increased to G = 480W/m^2 with a relatively constant temperature between 25^{0}C – 25.6^{0}C. The extracted power from one PV module and the waveform of the dc-link voltage is shown in Figure 12 (a)–(b), respectively. Figure 12(c) shows the output

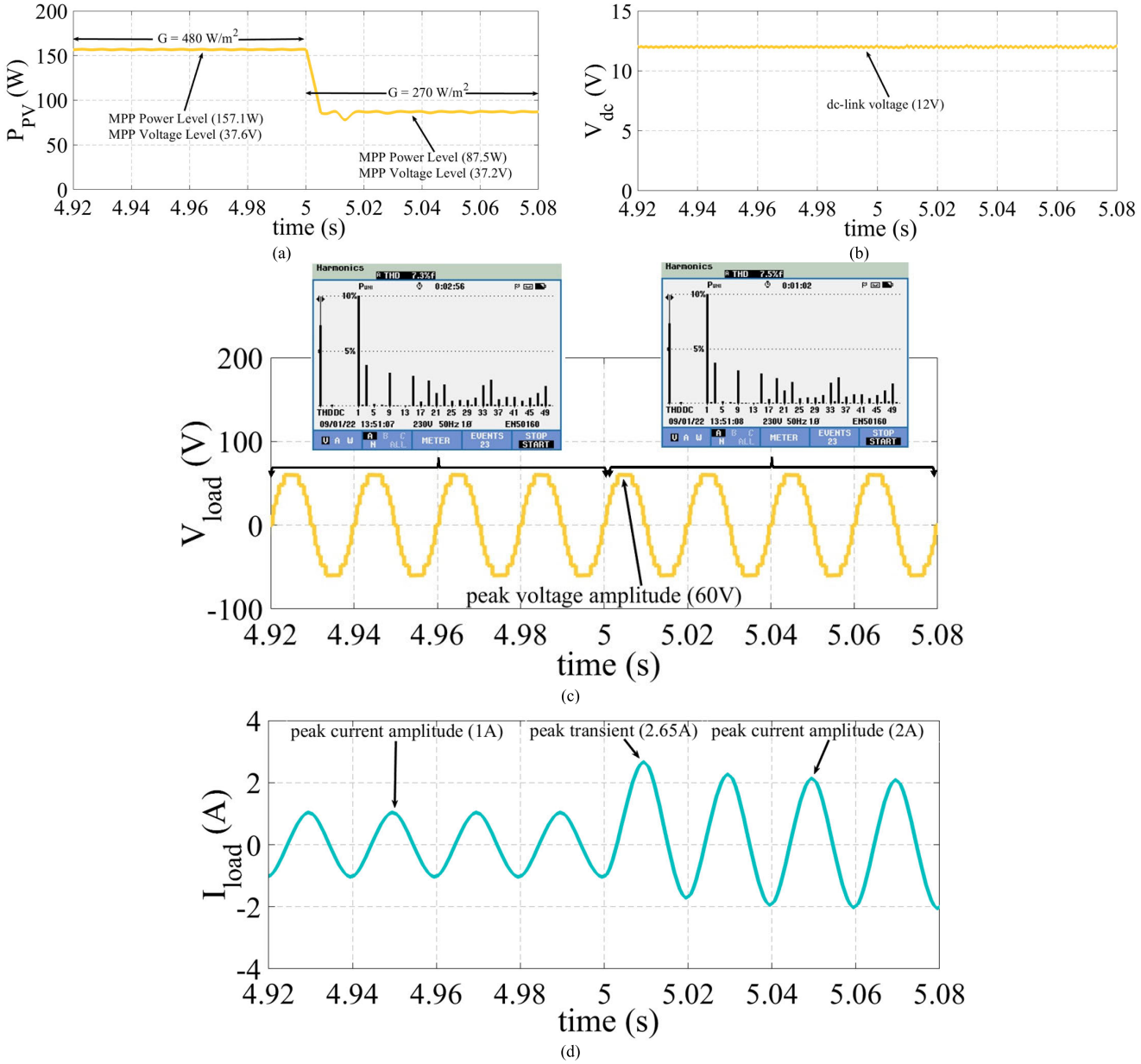

FIGURE 13. Zoomed Experimental waveforms of (a) PV module power, (b) dc-link capacitor voltage, (c) output voltage with its harmonic plot and (e) output current under simultaneous sudden change in irradiance and load.

voltage waveform under sudden change in irradiance. The meticulously designed MPPT controller helps in extracting the maximum power from the PV module when G varies from 270W/m^2 to 480W/m^2 as seen from Figure 12(a). Since the magnitude and shape of output voltage waveform is dependent on M, the variation of irradiance has no effect on the voltage waveform as evident from Figure 12(c). The harmonic profile of the voltage waveforms obtained at G = 270 W/m^2 and 480 W/m^2, respectively shows that the proposed SHE method effectively mitigates the dominant order harmonics during sudden change in irradiance. The load current remains unchanged as it is independent of the variation in irradiance levels as shown in Figure 12(d).

Case Study 2: Under simultaneous sudden change in irradiance and load

In the second experimental case study, the performance of the proposed SHE method is tested on 11-level MLI with standalone PV system under simultaneous sudden change in irradiance and load. The PV modules are operated with a starting irradiance of G = 480W/m^2 and a RL load with R = 10Ω and L = 200mH is connected to the 11-L MLI. At t = 5s, the irradiance and the load are instantly reduced to G = 270W/m^2 with R = 5Ω and L = 100mH with a relatively constant temperature between 25^{0}C – 25.6^{0}C. The power extracted from the PV module is shown in Figure 13 (a). The meticulously designed dc-link controller helps in maintaining

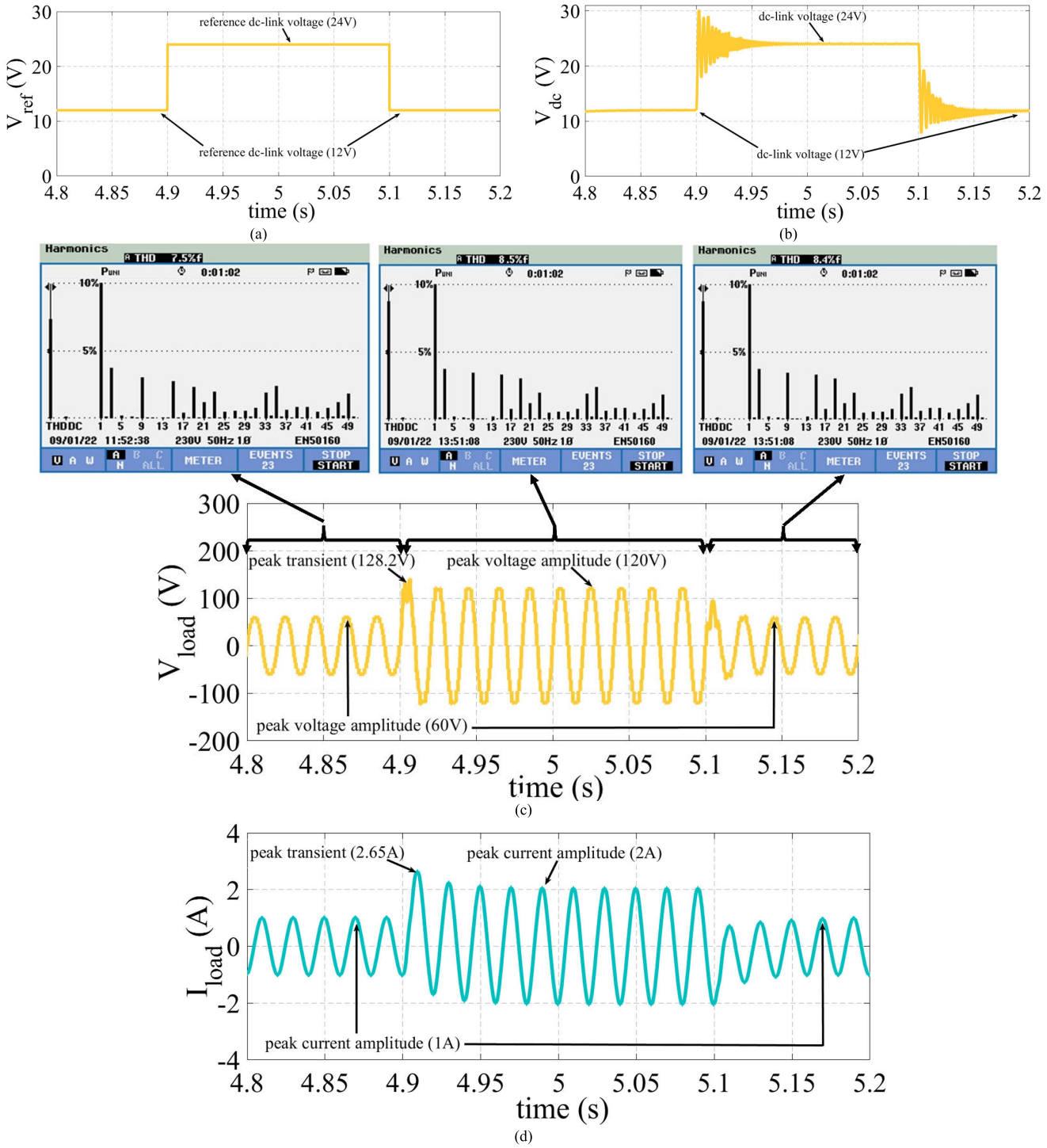

FIGURE 14. Zoomed Experimental waveforms of (a) reference dc-link capacitor voltage, (b) dc-link capacitor voltage, (c) output voltage with its harmonic plot and (e) output current under sudden change in the dc-link capacitor voltage.

a constant voltage of 12V as shown in Figure 13(b). The load voltage and current waveforms under simultaneous sudden change in irradiance and load are shown in Figure 13(c)–(d), respectively. Since, the magnitude and shape of output voltage waveform is dependent on the M, the variation of irradiance has no effect on the voltage waveform as evident from Figure 13(c).

However, the peak current amplitude is doubled as it depends on the load power which is doubled at t = 0.5s. The harmonic profile of voltage waveform using the proposed ASO SHE method effectively mitigates the dominant 5^{th}, 7^{th}, 11^{th}, and 13^{th} order harmonics during simultaneous sudden variation in irradiance and load as shown in Figure 13(c).

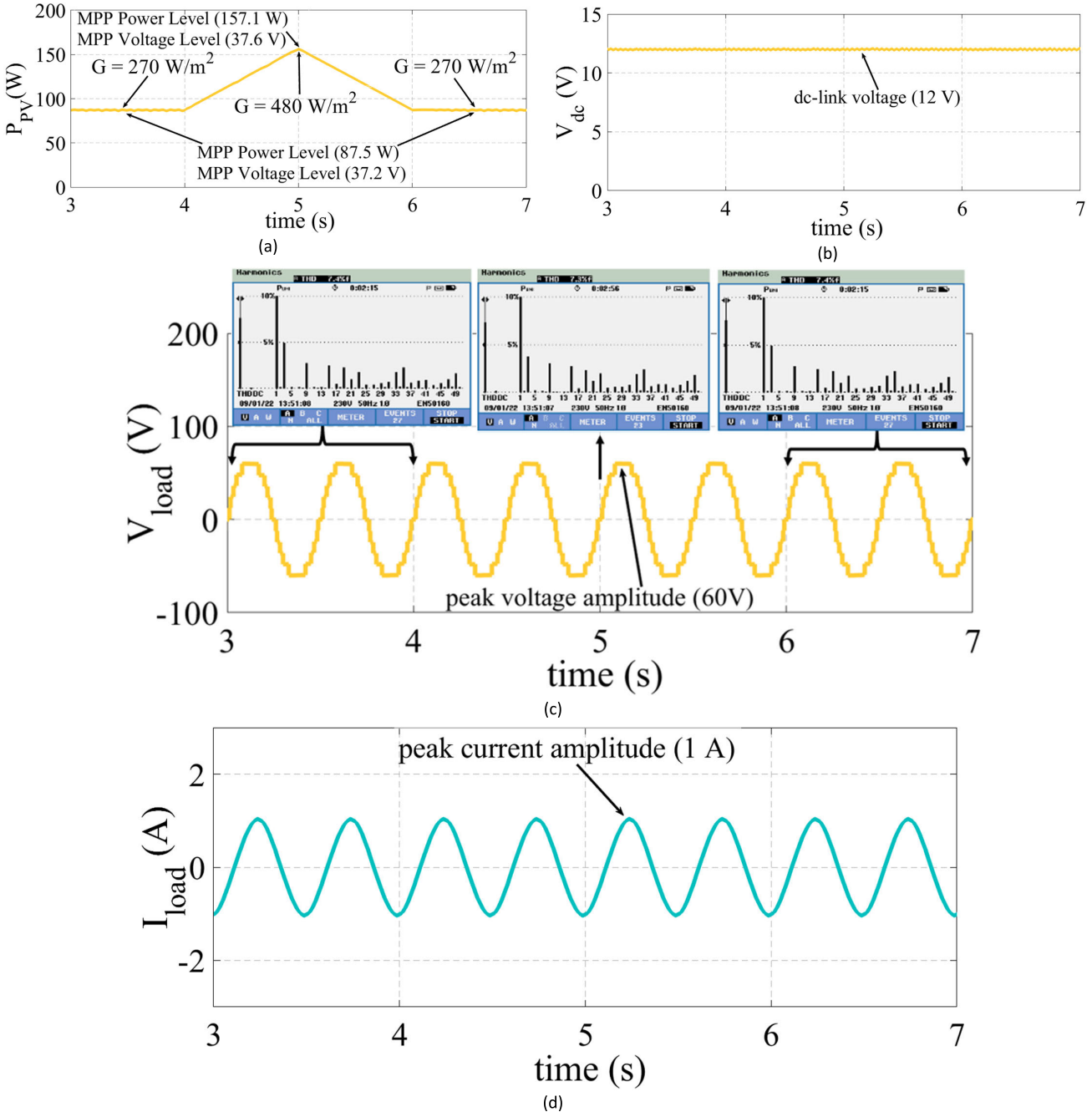

FIGURE 15. Zoomed waveforms of (a) PV module power, (b) dc-link capacitor voltage, (c) output voltage with its harmonic plot and (e) output current under ramp change in irradiance.

Case Study 3: Under sudden change in the dc-link capacitor voltage

In the third experimental case study, the performance of the proposed SHE method is tested under sudden change in the magnitude of the dc-link capacitors voltage. As mentioned earlier, there are five dc-link capacitors in the 11-level inverter. Initially, the reference value of the dc-link capacitor voltage is fixed at 12V. After some time at t = 4.9s, the reference value of the dc-link capacitor voltage is instantly changed to 24V. The reference value of the dc-link voltage is instantly reduced back to 12V at t = 5.1s as shown in Figure 14(a). The meticulously designed dc-link controller ensures that the dc-link capacitor voltage quickly settles to the new reference value with small transients as shown in Figure 14(b). The load voltage waveform under sudden change in dc-link voltage is shown in Figure 14(c). It can be seen that the magnitude of load voltage rises by twofold as the dc-link voltage is doubled at t = 4.9s. In a similar way, the magnitude of the load current also increased two-fold due to sudden increase in the dc-link capacitor voltage as shown in

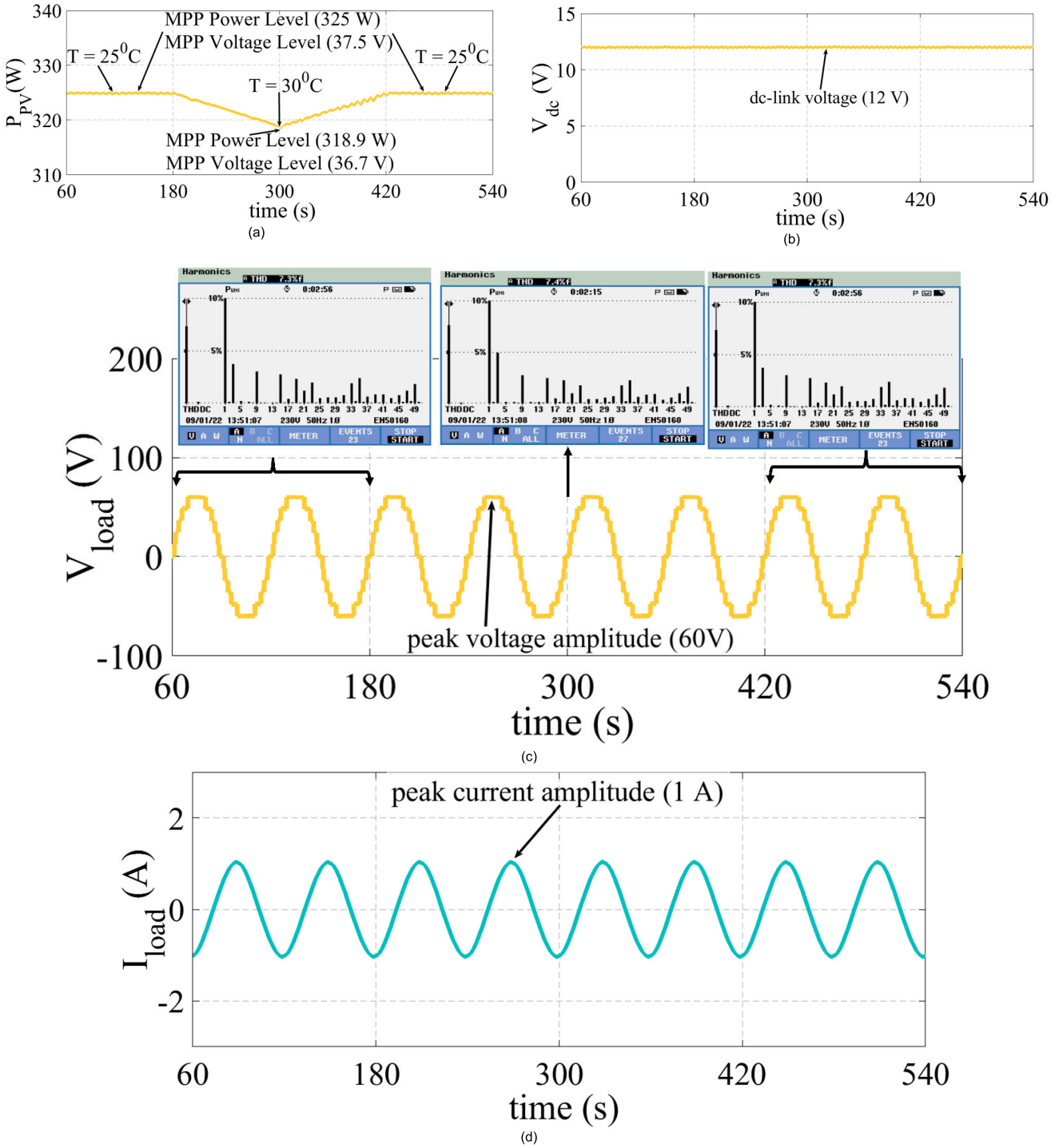

FIGURE 16. Zoomed waveforms of (a) PV module power, (b) dc-link capacitor voltage, (c) output voltage with its harmonic plot and (e) output current under ramp change in temperature.

Figure 14(d). It can be seen that the peak value of load current is 1 A when the dc-link voltage is 12V whereas the peak value of the load current increased to 2A when the dc-link voltage is increased to 24V. The harmonic profile of load voltage waveform shows that the proposed ASO effectively minimized the THD as well as 5th, 7th, 11th and 13th order harmonics under sudden variation in the dc-link capacitor voltage.

B. ROBUSTNESS AND STABILITY OF THE PROPOSED SHE METHOD UNDER CHANGES IN IRRADIANCE AND TEMPERATURE

To further assess the robustness and stability of the proposed SHE method, the authors have carried out two additional case studies. In the first case study the proposed SHE method is tested under ramp change in irradiance, whereas the second case study investigates the performance of the ASO-based

SHE method under dynamic change in temperature condition.

Case Study 1: Under ramp change in irradiance

In this case study, the irradiance is slowly increased from G = 270 W/m^2 at t = 4s to G = 480 W/m^2 at t = 5s and decreased from G = 480 W/m^2 at t = 6s with a relatively constant temperature between 25^{0}C – 25.6^{0}C. The 11-level multilevel inverter is operated at M = 0.75. The dc-link capacitor reference voltage is chosen as 12V and the 11-L MLI is connected to a constant load of R = 10Ω and L = 200mH. The power extracted from one PV module and the dc-link voltage waveforms are shown in Figure 15 (a)–(b), respectively. The output voltage waveform under ramp change in irradiance is shown in Figure 15 (c). The MPPT controller extracts the maximum power from the PV module during ramp change in irradiance from 270W/m^2 to 480W/m^2 and back to 270W/m^2 as seen from Figure 15 (a). As evident from Figure 15 (c), the variation of irradiance has no effect on the voltage waveform as the magnitude and shape of output voltage waveform is dependent on M. The harmonic profile of the voltage waveforms obtained at G = 270 W/m^2 and 480 W/m^2, respectively shows that the proposed SHE method effectively mitigates the dominant order harmonics during sudden change in irradiance as shown in Figure 15 (c). The load current remains unchanged as it is independent of the variation in irradiance levels as shown in Figure 15 (d).

Case Study 2: Under ramp change in temperature

In the second case study, the system is operated at G = 1000 W/m^2 while the temperature is gradually increased from T = 25^{0}C at t = 180s to T = 30^{0}C at t = 300s and decreased back to T = 25^{0}C at t = 420s. As the time constant of the temperature variation is sufficiently large the time taken for a 5^{0}C change in temperature is taken as 2 minutes. The dc-link capacitor reference voltage is chosen as 12V and the 11-L MLI is operated at M = 0.75 and connected to a constant load of R = 10Ω and L = 200mH. The PV module power and the dc-link voltage waveforms are shown in Figure 16 (a)–(b), respectively. The output voltage waveform under ramp change in temperature is shown in Figure 16 (c). The MPPT controller extracts the maximum power from the PV module during slow change in temperature from 25^{0}C to 30^{0}C and back to 25^{0}C as seen from Figure 16 (a). As evident from Figure 16 (c), the variation of temperature has no effect on the voltage waveform as the magnitude and shape of output voltage waveform is dependent on the modulation index. The harmonic profile of the voltage waveforms obtained at T = 25^{0}C and T = 30^{0}C, respectively shows that the proposed SHE method effectively mitigates the dominant order harmonics during ramp change in temperature as shown in Figure 16 (c). The load current remains unchanged as it is independent of the variation in temperature as shown in Figure 16 (d).

VII. CONCLUSION

In this research paper, ASO based SHE method is proposed to effectively minimize the THD and detrimental harmonics (5th, 7th, 11th, and 13th) present in the load voltage waveform of PV based 11-level MLI for dynamic operating conditions. From detailed simulation and comparative studies, it is determined that the ASO based SHE method performed better than bee, firefly, PSO, TLBO and ICA based SHE methods in terms of CDF, rate of convergence, and optimum fitness values for wide range of M in five-dimension SHE problem. Three case scenarios are investigated to effectively demonstrate the performance of the proposed ASO SHE method. In the first case scenario, the proposed SHE method is tested under sudden change in irradiance. The results indicate that the dominant harmonics are effectively minimized and the THD remained well below the specified limits as per IEEE-519-2022 standard. In the scenario, the proposed method is tested under simultaneous sudden changes in irradiance and load condition. The simulation results exhibit low THD in the load voltage by reducing the dominant harmonics which confirms the desired objectives of the proposed SHE method. The third case scenario evaluates the performance of the ASO SHE method under sudden change in the reference value of the dc-link capacitor voltage. The results illustrate small distortion in the load voltage during transient state which marginally increases the THD of the voltage waveform. The experimental results confirm that the proposed SHE method and the meticulously designed dc-link voltage controller performed well under sudden change in irradiance, load and dc-link voltage. In the near future, the proposed SHE method will be tested on different grid connected MLI topologies.

ACKNOWLEDGMENT

Views and opinions expressed are however those of the author(s) only and do not necessarily reflect those of the European Union and/or UKRI. Neither the European Union nor UKRI nor the granting authority can be held responsible for them.

REFERENCES

[1] R. Agrawal and S. Jain, "Comparison of reduced part count multilevel inverters (RPC-MLIs) for integration to the grid," *Int. J. Electr. Power Energy Syst.*, vol. 84, pp. 214–224, Jan. 2017.
[2] P. Kala and S. Arora, "A comprehensive study of classical and hybrid multilevel inverter topologies for renewable energy applications," *Renew. Sustain. Energy Rev.*, vol. 76, pp. 905–931, Sep. 2017.
[3] M. S. A. Dahidah, G. Konstantinou, and V. G. Agelidis, "A review of multilevel selective harmonic elimination PWM: Formulations, solving algorithms, implementation and applications," *IEEE Trans. Power Electron.*, vol. 30, no. 8, pp. 4091–4106, Aug. 2015.
[4] M. Ahmed, "General mathematical solution for selective harmonic elimination," *IEEE J. Emerg. Sel. Topics Power Electron.*, vol. 8, no. 4, pp. 4440–4456, Dec. 2020.
[5] M. A. Memon, S. Mekhilef, M. Mubin, and M. Aamir, "Selective harmonic elimination in inverters using bio-inspired intelligent algorithms for renewable energy conversion applications: A review," *Renew. Sustain. Energy Rev.*, vol. 82, pp. 2235–2253, Feb. 2018.
[6] H. Taghizadeh and M. T. Hagh, "Harmonic elimination of cascade multilevel inverters with nonequal DC sources using particle swarm optimization," *IEEE Trans. Ind. Electron.*, vol. 57, no. 11, pp. 3678–3684, Nov. 2010.
[7] A. Kavousi, B. Vahidi, R. Salehi, M. K. Bakhshizadeh, N. Farokhnia, and S. H. Fathi, "Application of the bee algorithm for selective harmonic elimination strategy in multilevel inverters," *IEEE Trans. Power Electron.*, vol. 27, no. 4, pp. 1689–1696, Apr. 2012.

[8] M. H. Etesami, N. Farokhnia, and S. H. Fathi, "Colonial competitive algorithm development toward harmonic minimization in multilevel inverters," *IEEE Trans. Ind. Informat.*, vol. 11, no. 2, pp. 459–466, Apr. 2015.
[9] M. H. Etesami, D. M. Vilathgamuwa, N. Ghasemi, and D. P. Jovanovic, "Enhanced metaheuristic methods for selective harmonic elimination technique," *IEEE Trans. Ind. Informat.*, vol. 14, no. 12, pp. 5210–5220, Dec. 2018.
[10] M. G. Sundari, M. Rajaram, and S. Balaraman, "Application of improved firefly algorithm for programmed PWM in multilevel inverter with adjustable DC sources," *Appl. Soft Comput.*, vol. 41, pp. 169–179, Apr. 2016.
[11] S. S. Lee, B. Chu, N. R. N. Idris, H. H. Goh, and Y. E. Heng, "Switched-battery boost-multilevel inverter with GA optimized SHEPWM for standalone application," *IEEE Trans. Ind. Electron.*, vol. 63, no. 4, pp. 2133–2142, Apr. 2016.
[12] P. K. Kar, A. Priyadarshi, and S. B. Karanki, "Selective harmonics elimination using whale optimisation algorithm for a single-phase-modified source switched multilevel inverter," *IET Power Electron.*, vol. 12, no. 8, pp. 1952–1963, Jul. 2019.
[13] M. A. Memon, S. Mekhilef, and M. Mubin, "Selective harmonic elimination in multilevel inverter using hybrid APSO algorithm," *IET Power Electron.*, vol. 11, no. 10, pp. 1673–1680, Aug. 2018.
[14] A. N. Kumle, S. H. Fathi, F. Jabbarvaziri, M. Jamshidi, and S. S. H. Yazdi, "Application of memetic algorithm for selective harmonic elimination in multi-level inverters," *IET Power Electron.*, vol. 8, no. 9, pp. 1733–1739, Sep. 2015.
[15] K. Haghdar, "Optimal DC source influence on selective harmonic elimination in multilevel inverters using teaching–learning-based optimization," *IEEE Trans. Ind. Electron.*, vol. 67, no. 2, pp. 942–949, Feb. 2020.
[16] P. Kala and S. Arora, "Implementation of hybrid GSA SHE technique in hybrid nine-level inverter topology," *IEEE J. Emerg. Sel. Topics Power Electron.*, vol. 9, no. 1, pp. 1064–1074, Feb. 2021.
[17] Y. Gopal, Y. N. V. Kumar, A. Kumari, O. Prakash, S. Chowdhury, and A. A. Almehizia, "Reduced device count for self balancing switched-capacitor multilevel inverter integration with renewable energy source," *Sustainability*, vol. 15, no. 10, p. 8000, May 2023.
[18] S. Dhara and V. T. Somasekhar, "A nine-level transformerless boost inverter with leakage current reduction and fractional direct power transfer capability for PV applications," *IEEE J. Emerg. Sel. Topics Power Electron.*, vol. 10, no. 6, pp. 7938–7949, Dec. 2022, doi: 10.1109/JESTPE.2021.3074701.
[19] X. Zhu, H. Wang, W. Zhang, H. Wang, X. Deng, and X. Yue, "A novel single-phase five-level transformer-less photovoltaic (PV) inverter," *CES Trans. Electr. Mach. Syst.*, vol. 4, no. 4, pp. 329–338, Dec. 2020.
[20] H. Vahedi, M. Sharifzadeh, and K. Al-Haddad, "Modified seven-level pack U-cell inverter for photovoltaic applications," *IEEE J. Emerg. Sel. Topics Power Electron.*, vol. 6, no. 3, pp. 1508–1516, Sep. 2018.
[21] S. Ramaiah, N. Lakshminarasamma, and M. K. Mishra, "Multisource switched capacitor based boost multilevel inverter for photovoltaic-based systems," *IEEE Trans. Power Electron.*, vol. 35, no. 3, pp. 2558–2570, Mar. 2020.
[22] H. Nademi, A. Das, R. Burgos, and L. E. Norum, "A new circuit performance of modular multilevel inverter suitable for photovoltaic conversion plants," *IEEE J. Emerg. Sel. Topics Power Electron.*, vol. 4, no. 2, pp. 393–404, Jun. 2016.
[23] Y. Gopal, D. Birla, and M. Lalwani, "Reduced switches multilevel inverter integration with boost converters in photovoltaic system," *SN Appl. Sci.*, vol. 2, pp. 1–15, Jan. 2020.
[24] Y. Gopal, K. P. Panda, and D. Birla, "Genetic algorithm and anti-predatory swarm optimisation-based solutions for selective harmonic elimination in multilevel inverters," *Int. J. Power Electron.*, vol. 15., nos. 3–4, pp. 290–308, Apr. 2022.
[25] Y. Gopal, K. P. Panda, Y. N. V. Kumar, and G. V. Pradeep, "Reduction in harmonics for PV-based reduced device count multilevel inverter with genetic algorithm," in *Sustainable Energy Technological Advancements*. Singapore: Springer, 2022.
[26] R. R. Karasani, V. B. Borghate, P. M. Meshram, H. M. Suryawanshi, and S. Sabyasachi, "A three-phase hybrid cascaded modular multilevel inverter for renewable energy environment," *IEEE Trans. Power Electron.*, vol. 32, no. 2, pp. 1070–1087, Feb. 2017.
[27] G. V. Bharath, A. Hota, and V. Agarwal, "A new family of 1-f five-level transformerless inverters for solar PV applications," *IEEE Trans. Ind. Appl.*, vol. 56, no. 1, pp. 561–569, Jan. 2020.
[28] K. P. Panda, S. S. Lee, and G. Panda, "Reduced switch cascaded multilevel inverter with new selective harmonic elimination control for standalone renewable energy system," *IEEE Trans. Ind. Appl.*, vol. 55, no. 6, pp. 7561–7574, Nov. 2019.
[29] W. Zhao, L. Wang, and Z. Zhang, "Atom search optimization and its application to solve a hydrogeologic parameter estimation problem," *Knowl.-Based Syst.*, vol. 163, pp. 283–304, Jan. 2019.
[30] *IEEE Standard for Harmonic Control in Electric Power Systems*, Standard 519-2022 (Revision of IEEE Std 519-2014), Aug. 2022, pp. 1–31.
[31] G.-J. Su, "Multilevel DC-link inverter," *IEEE Trans. Ind. Appl.*, vol. 41, no. 3, pp. 848–854, May 2005.
[32] E. Babaei, S. Laali, and S. Alilu, "Cascaded multilevel inverter with series connection of novel H-bridge basic units," *IEEE Trans. Ind. Electron.*, vol. 61, no. 12, pp. 6664–6671, Dec. 2014.
[33] M. Ali, M. Tariq, R. K. Chakrabortty, M. J. Ryan, B. Alamri, and M. A. Bou-Rabee, "11-level operation with voltage-balance control of WE-type inverter using conventional and DE-SHE techniques," *IEEE Access*, vol. 9, pp. 64317–64330, 2021.
[34] M. Ali, M. Tariq, A. Sarwar, and B. Alamri, "A 13-, 11-, and 9-level boosted operation of a single-source asymmetrical inverter with hybrid PWM scheme," *IEEE Trans. Ind. Electron.*, vol. 69, no. 12, pp. 12817–12828, Dec. 2022.
[35] S. S. Lee, S. Member, C. S. Lim, K. Lee, and S. Member, "Novel active-neutral-point-clamped inverters with improved voltage-boosting capability," *IEEE Trans. Power Electron.*, vol. 35, no. 6, pp. 5978–5986, Jun. 2020.
[36] A. Routray, R. K. Singh, and R. Mahanty, "Harmonic reduction in hybrid cascaded multilevel inverter using modified grey wolf optimization," *IEEE Trans. Ind. Appl.*, vol. 56, no. 2, pp. 1827–1838, Mar. 2020.
[37] V. Jately, S. Bhattacharya, B. Azzopardi, A. Montgareuil, J. Joshi, and S. Arora, "Voltage and current reference based MPPT under rapidly changing irradiance and load resistance," *IEEE Trans. Energy Convers.*, vol. 36, no. 3, pp. 2297–2309, Sep. 2021.
[38] M. A. Memon, M. D. Siddique, S. Mekhilef, and M. Mubin, "Asynchronous particle swarm optimization-genetic algorithm (APSO-GA) based selective harmonic elimination in a cascaded H-bridge multilevel inverter," *IEEE Trans. Ind. Electron.*, vol. 69, no. 2, pp. 1477–1487, Feb. 2022.

PEEYUSH KALA (Member, IEEE) was born in Pauri Garhwal, India, in April 1987. He received the B.Tech. degree from Uttarakhand Technical University, Dehradun, India, in 2010, and the M.Tech. degree in electrical energy systems and the Ph.D. degree in electrical engineering from the Govind Ballabh Pant University of Agriculture and Technology, Pantnagar, India, in 2012 and 2018, respectively. He was an Assistant Professor with the Department of Electrical and Electronics Engineering, Shivalik College of Engineering, Dehradun, and the Department of Electrical Engineering, Women Institute of Technology, Dehradun. He is currently with the Department of Electrical and Electronics Engineering, SRM Institute of Science and Technology, Delhi-NCR Campus, Ghaziabad, India. He has completed one funded research project on the development of a hybrid multilevel inverter topology for distributed energy sources. He has published papers and book chapters in peer-reviewed journals and conferences in the field of power electronics. His research interests include multilevel inverters, optimization techniques, and photovoltaic systems. He is also an Active Reviewer for reputed journals, such as IEEE TRANSACTIONS ON INDUSTRIAL ELECTRONICS, *IET Power Electronics*, and IEEE TRANSACTIONS ON INDUSTRY APPLICATIONS.

VIBHU JATELY (Senior Member, IEEE) received the Ph.D. degree from G. B. Pant University, Pantnagar, India. He was an Assistant Professor under the United Nations Development Program with the Department of Electrical and Computer Engineering, Wollo University, Ethiopia. He was a Postdoctoral Research Fellow for two years with the MCAST Energy Research Group, Malta, where he was the Task Leader of European H2020 Projects. He is currently an Assistant Professor (Selection Grade) with the Department of Electrical and Electronics Engineering, University of Petroleum and Energy Studies, Dehradun, India. He has over eight years of teaching and research experience. His area of interest includes power electronics applications in renewable energy systems and has worked on formulating MPPT algorithms, control strategies for grid integration of PVs, microgrids, and the use of AI techniques in PV applications.

ABHINAV SHARMA received the B.Tech. degree from H. N. B. Garhwal University, Srinagar, India, in 2009, and the M.Tech. and Ph.D. degrees from the Govind Ballabh Pant University of Agriculture and Technology, Pantnagar, India, in 2011 and 2016, respectively. He is currently an Assistant Professor (Selection Grade) with the Department of Electrical and Electronics Engineering, University of Petroleum and Energy Studies, Dehradun. He has published a number of research articles in journals and conferences. His research interests include adaptive array signal processing, smart antennas, artificial intelligence, and machine learning.

JYOTI JOSHI received the B.Tech. degree in electrical and electronics engineering from Uttarakhand Technical University (UTU), India, in 2011, the M.Tech. degree from IFTM University, India, in 2015, and the Ph.D. degree in electrical engineering from the G. B. Pant University of Agriculture and Technology, Pantnagar. She is currently an Assistant Professor with the Department of Computer Science and Engineering, Graphic Era Hill University, Dehradun. She has over eight years of teaching experience during which she also served as a Lecturer under the United Nations Development Programme in Ethiopia. Her research interests include current controllers in grid-connected photovoltaic systems, fault ride-through in grid-connected photovoltaic systems, and flexible power point tracking techniques in photovoltaic systems.

BRIAN AZZOPARDI (Senior Member, IEEE) received the B.Eng. degree from the University of Malta, Msida, Malta, in 2002, and the Ph.D. degree from The University of Manchester, Manchester, U.K., in 2011. He is currently a Senior Academician with the Malta College of Arts, Science, and Technology, Paola, Malta, and leads the Energy Research Group, and a Visiting Senior Lecturer with the University of Malta. His research interests include photovoltaics and electric mobility network integration and future urban low-carbon society.